JGR Solid Earth

RESEARCH ARTICLE
10.1029/2019JB019010

Key Points:
- Coulomb stress analysis of large mainshocks in central Taiwan from 1900 to 2017 reveals that five events were promoted and seven were inhibited
- Coseismic energy release during preceding earthquakes promoted rupture propagation of the 1941 Chungpu, 1998 Rueyli, and 1999 Chi-Chi earthquakes
- The Chukou, Chishan, and Chaochou faults and flat decollement of central Taiwan were promoted by coseismic slip of $M_L \geq$ 5.5 earthquakes

Supporting Information:
- Supporting Information S1
- Figure S1
- Figure S2

Correspondence to:
S. Li,
shli@fiu.edu

Citation:
Li, S., Wdowinski, S., Hsu, Y.-J., Shyu, J. B. H. (2020). Earthquake interactions in central Taiwan: Probing Coulomb stress effects due to $M_L \geq$ 5.5 earthquakes from 1900 to 2017. *Journal of Geophysical Research: Solid Earth*, *125*, e2019JB019010. https://doi.org/10.1029/2019JB019010

Received 6 NOV 2019
Accepted 13 JUL 2020
Accepted article online 20 JUL 2020

Earthquake Interactions in Central Taiwan: Probing Coulomb Stress Effects Due to $M_L \geq$ 5.5 Earthquakes From 1900 to 2017

Shanshan Li[1], Shimon Wdowinski[1], Ya-Ju Hsu[2], and J. Bruce H. Shyu[3]

[1]Institute of Environment, Department of Earth and Environment, Florida International University, Miami, FL, USA, [2]Institute of Earth Sciences, Academia Sinica, Nankang, Taiwan, [3]Department of Geosciences, National Taiwan University, Taipei, Taiwan

Abstract Though large efforts have been made in studying earthquake generation processes, earthquake triggering in central Taiwan is still not well understood. The occurrence of 14 mainshocks with $M_L \geq$ 6.0 from 1900 to 2017 and the presence of eight active fault systems provide excellent data sets for studying earthquake interaction in central Taiwan. We examined the coseismic Coulomb stress changes (ΔCFSs) due to mainshocks in the sequence and other surrounding earthquakes comprising 3 smaller magnitude mainshocks with 5.5 $\leq M_L \leq$ 6.0 and 25 aftershocks with $M_L \geq$ 5.5. When considering only triggering effects from mainshocks in the sequence, the compounded ΔCFSs are significant for all 13 mainshocks with 8 being promoted (ΔCFS > 0.1 bar) and 5 being inhibited (ΔCFS < −0.1 bar). After adding effects from other surrounding earthquakes, we found that five mainshocks were promoted and seven were inhibited. Yet it is questionable whether the 2016 mainshock was promoted, because the calculated uncertainties at the hypocenter might reduce ΔCFS below the 0.1 bar triggering threshold. In addition, significant positive ΔCFSs (>2 bars) on the Chukou, Chaochou, and Chishan faults and flat decollement of central Taiwan suggest failure promotion on those active faults. Contrarily, significant negative ΔCFSs (<−0.2 bar) on the Changhua, Shungtung, Chelungpu, and Hsinhua faults suggest that ruptures on those faults might be inhibited. We also conducted sensitivity studies indicating uncertainty level of 33–38% of the calculated ΔCFSs. Our findings indicate that preceding earthquakes have affected nucleation and rupture propagation of large earthquakes in central Taiwan during the past 120 years.

1. Introduction

Taiwan is a tectonic active island where collision processes absorb deformation occurring between two neighboring subduction systems (Figure 1a). In the offshore northeast of Taiwan, the Philippine Sea plate subducts northward beneath the Eurasian plate along the Ryukyu Trench. In southern Taiwan, the South China Sea of the Eurasian plate subducts eastward beneath the Philippine sea plate along the Manila trench. The present-day plate convergence rate between the Luzon Volcanic Arc and the Chinese continental passive margin is 83–90 mm/year (Hsu et al., 2016) (Figure 1). Active collision, which connects the two subduction systems, occurs between the Luzon volcanic arc and Chinese continent passive margins. Such complex and active tectonics result in intense seismic activity along the plate boundary regions, mountain fronts, and inland active faults in Taiwan. High-quality records of the seismic activity provide us a valuable opportunity to study the physical mechanism beneath the occurrence and propagation of large earthquakes.

The high rate of seismic activity in Taiwan reflects the rapid convergence between the Philippine Sea and Eurasian plates, which is absorbed on land by active faults and the northward subduction of the Philippine Sea Plate under the Eurasian plate (Wu, 1978; Wu et al., 2007). Specifically, central Taiwan is frequently affected by moderate and large magnitude earthquakes, as indicated by 42 $M_L \geq$ 5.5 of which occurred between 1900 and 2017. Within these earthquakes, we identified 14 mainshocks with $M_L \geq$ 6.0. Those 14 large earthquakes occurred on or near the inland active faults systems in the central mountainous area (Figure 1b and Table 1), hereinafter termed the Central-Taiwan-Mainshock earthquake sequence. These large magnitude earthquakes demonstrate the need for earthquake hazard assessment and underscore the imperative to prepare for the next large main shock in central Taiwan. Answering the question of whether these large magnitude mainshocks were triggered by their preceding earthquakes may provide

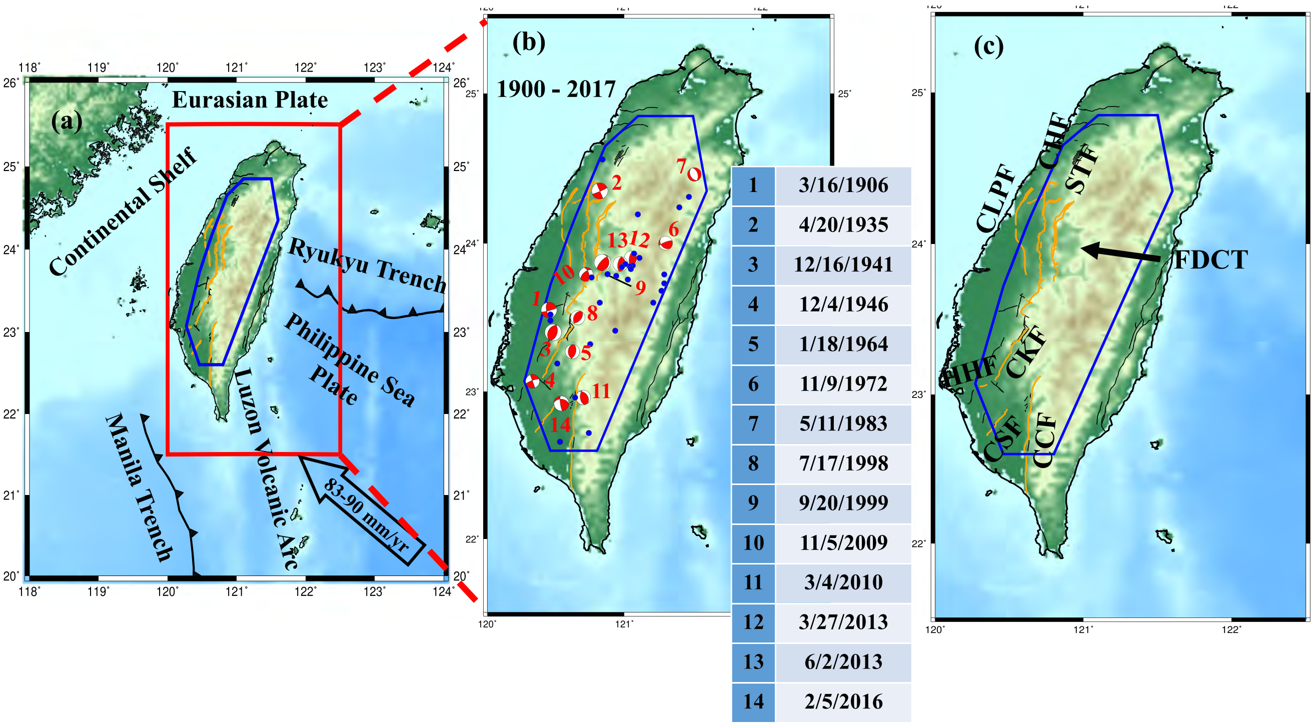

Figure 1. (a) Tectonic map of Taiwan. The plate convergence rate 83–90 mm/year is from Hsu et al. (2016). (b) Earthquakes and active faults used in this study. The blue outline marks our area of interest. Red beach balls represent large mainshocks with $M_L \geq 6.0$ from 1900 to 2017 (the Central-Taiwan-Mainshock sequence). Blue points represent surrounding earthquakes with $M_L \geq 5.5$ including mainshocks. Black lines mark active faults of Taiwan (Hsu et al., 2016), and black bold texts show the active faults studied in this paper. CHF: Changhua fault; CLPF: Chelungpu fault; STF: Shungtung fault; FDCT: flat decollement of central Taiwan; CKF: Chukou fault; HHF: Hsinghua fault; CCF: Chaochou fault; CSF: Chishan fault.

Table 1
Occurrence Times, Hypocenters, Source Mechanisms, and Moment Magnitudes of the 14 Mainshocks in the Central-Taiwan-Mainshock Earthquake Sequence

Event		Hypocenter			Source mechanisms				
Date	Name	Longitude (deg)	Latitude (deg)	Depth (km)	Strike (deg)	Dip (deg)	Rake (deg)	Ml	Reference
1906/3/16	Meishan	120.45	23.55	6	75	85	153	6.9	Liao et al. (2018)
1935/4/20	Hsinchu	120.82	24.35	5	67	85	180	7.1	Lin et al. (2013)
1941/12/16	Chungpu	120.48	23.40	12	15	50	80	7.3	Lin & Xiao (2004)
1946/12/4	Hsinhua	120.33	23.07	5	250	80	180	6.1	Hsu et al. (2011)
1964/1/18	Baihe	120.62	23.27	18	15	50	100	6.3	CWBSN and Kao et al. (2000)
1972/11/9	Hualien	121.3	24	10	137	33	155	6.1	CWBSN and Wu (1978)
1983/5/11	Taiping-shan	121.51	24.46	1.23	150	40	−100	6.0	CWBSN and CMT
1998/7/17	Rueyli	120.66	23.50	2.8	40	50	100	6.2	CWBSN and Ma & Wu (2001)
1999/9/20	Chi-Chi	120.84	23.87	8.0	5	23	55	7.3	Johnson et al. (2001)
2009/11/5	Nantou	120.72	23.79	24.08	230	59	139	6.2	CWBSN and CMT
2010/3/4	Jiashian	120.7	22.96	22.43	324	39	67	6.4	CWBSN and Hsu et al. (2011)
2013/3/27	Nantou	121.05	23.90	19.4	355	25	75	6.2	Lee et al. (2015)
2013/6/2	Nantou	120.97	23.86	14.5	2	29	83	6.5	Lee et al. (2015)
2016/2/5	Meinong	120.54	22.92	15.3	275	42	17	6.6	CWBSN anad Wen et al. (2017)

Note. Those parameters define the receiver faults for the first Coulomb tress analysis. Date format is yyyy/mm/dd. "CWBSN" in the reference list indicates the location of the mainshock obtained from the Central Weather Bureau Seismic Network. "CMT" indicates the focal mechanism information obtained from the global Centroid-Moment-Tensor (CMT) catalog for specific mainshock.

evidence and a linkage between earthquake triggering and interactions among active faults (Steacy et al., 2005).

The influence of static stress transfer from one or more large earthquakes on aftershocks or subsequent mainshocks, which is referred to as earthquake interaction, was demonstrated in previous studies using the Coulomb failure model (Freed, 2005; King et al., 1994). Earthquake triggering can occur in short time scales, such as the mainshock-aftershock interaction (Stein et al., 1992), or long time scales, like mainshock-mainshock interaction (Price & Bürgmann, 2002). Such stress transfer among earthquakes can happen in nearby region (Ishibe et al., 2015) or at greater distances (Hough et al., 2002).

Large earthquakes of the Central-Taiwan-Mainshock sequence were successfully used to study several aspects of earthquake interactions. Most studies focused on the 1999 M_L 7.3 Chi-Chi earthquake and its impact on the nearby seismic activity, in terms of (1) changes in seismicity after the earthquake (Ma et al., 2005), (2) mainshock-aftershock interactions (Chan & Stein, 2009), (3) mainshock-mainshock interactions (Chan & Wu, 2014), and (4) stress triggering among earthquakes with respect to postseismic induced deformation (Chan & Stein, 2009). Potential effect on subsequent aftershocks, surrounding active faults, and local seismic zone due to mainshock rupture has also been explored for the 1935 M_L 7.1 Hsinchu mainshock (Lin et al., 2013). Additional studies of mainshock-aftershock interactions have been conducted for the 2010 Jiashian (Chan & Wu, 2012), the two 2013 Nantou, (Liao & Huang, 2016), and 2016 Meinong earthquakes (Wen et al., 2017). Hsu et al. (2011) explored the static stress transfer from coseismic rupture on active faults induced by the 2010 Jiashian earthquake. In general, those studies mostly focused on Coulomb stress triggering effects induced by a limited number of large earthquakes within a short time period.

In this study we explore the earthquake interaction effects in central Taiwan through estimating (1) Coulomb stress changes caused by preceding events on fault planes of subsequent mainshocks to evaluate whether the nucleation of those large earthquakes was promoted or inhibited and (2) Coulomb stress changes due to previous events on nearby fault systems and rupture planes of subsequent mainshocks to evaluate whether they promote or inhibit rupture propagation of mainshocks in the sequence or nucleation of future large earthquake. We focus on coseismic Coulomb stress changes induced by preceding earthquakes although other sources of stress such as postseismic Coulomb stress changes (Tang et al., 2019), dynamic stress changes (Gomberg et al., 2001), and secondary stress changes (Meier et al., 2014) may also matter. Specifically, in the first aspect, we consider stress triggering effects on the mainshocks from mainshocks themselves, as well as from other surrounding earthquakes including smaller magnitude mainshocks with $5.5 \leq M_L \leq 6.0$ and aftershocks with $M_L \geq 5.5$ separated based on the declustering algorithm of Gardner and Knopoff (1974). This systematic long-term earthquake analysis differs from merely analyzing triggering effects for a few earthquakes as previous studies did. It provides new insights on how preceding earthquakes can impact the nucleation of those large mainshocks that sequentially from 1900 to 2017 in central Taiwan. Based on historical records, the most destructive earthquakes in Taiwan were closely related to inland active faults. For instance, the 1999 M_L 7.3 Chi-Chi earthquake was attributed to the rupture of the Chelungpu fault (CLPF in Figure 1b). This large mainshock was fatal and caused significant life and financial losses. Thus, probing changes in stress field for active faults can be helpful in earthquake hazard mitigation. For the second aspect of our study, Coulomb stress effects on inland active faults due to preceding events have been explored. Thus, we are able to investigate whether rupture propagation of recent large mainshocks can be explained using the Coulomb failure model. In addition, the likelihood of future potential large earthquakes is also assessed through analysis of those preexisting earthquakes.

2. Method and Data

2.1. Method: The Coulomb Failure Model

Our earthquake interaction study is based on a Coulomb failure stress change (ΔCFS) analysis between two faults: source fault and receiver fault. Source faults are faults that release stress during coseismic rupture of earthquakes, which are usually calculated through coseismic slip models, while receiver faults are faults that receive stress from earthquakes. Stress changes induced by a source fault are calculated using the Okada elastic half-space dislocation model (Okada, 1992). We used a shear modulus of 3.3×10^4 MPa, in a uniform elastic half-space with Poisson's ratio of 0.25 (King et al., 1994). The calculated stress tensor changes are projected onto the observed orientation of the receiver fault and then decomposed into shear stress change ($\Delta\tau$) and normal stress change ($\Delta\sigma$) with respect to the fault surface to estimate the ΔCFS. The Coulomb failure model is as follows (King et al., 1994):

$$\Delta \mathrm{CFS} = \Delta\tau - \mu'\Delta\sigma \tag{1}$$

where μ' is the apparent coefficient of friction, which is defined as $\mu' = \mu(1 - B)$, where B is Skempton's coefficient related to induced pore pressure change and μ is the coefficient of friction. $\Delta\tau$ is assumed positive in the fault slip direction on a given failure plane and $\Delta\sigma$ is assumed positive in the compressive direction. Based on a previous study in Taiwan (Hsu et al., 2010), we chose $\mu' = 0.4$. According to the Coulomb failure criterion, a positive ΔCFS promotes receiver fault failure due to the source slip; a negative ΔCFS means preceding earthquakes reduces the chance of failure on those receiver faults. In this study, we used a triggering threshold of 0.1 bar (Ishibe et al., 2015), in which a ΔCFS greater than 0.1 bar significantly promotes earthquakes to failure. In addition, a ΔCFS less than −0.1 bar is considered to play a vital rule in inhibiting earthquakes to failure. ΔCFS values in the range of −0.1 to 0.1 are considered inconclusive for determining earthquake interaction effects.

2.2. Earthquake Data and Active Faults

The short-period, broadband, and strong-motion seismic networks operated by the Central Weather Bureau Seismic Network (CWBSN) (Institute of Earth Sciences, 1996) record about 18,000 earthquakes annually in a roughly 220,000 km^2 region in Taiwan (Wu, Chang, et al., 2008). The CWBSN was established in Taiwan since 1990s, which includes observation stations widely distributed over Taiwan (Wu, Chang, et al., 2008). In this study, we used earthquakes with $M_L \geq 5.5$ recorded in the Taiwan earthquake catalog (TEC) compiled by CWB located within central Taiwan (blue outline shown in Figure 1b) for the period 1900 to 2017. We are interested in central Taiwan because it is a seismic active region with abundant records of seismic events, which provides sufficient information to investigate earthquake interaction effects. The reason for using events with $M_L \geq 5.5$ is that smaller magnitude earthquakes have negligible impact on earthquake interaction because they induce very localized and low magnitude Coulomb stress changes. The TEC catalog includes 42 large and moderate earthquakes with $M_L \geq 5.5$ in central Taiwan. We identified 14 strong mainshocks with $M_L \geq 6.0$ (red beach balls in Figure 1b) using the declustering algorithm of Gardner and Knopoff (1974); we termed these 14 events as the Central-Taiwan-Mainshock sequence. The remaining earthquakes (blue dots in Figure 1b) were classified as surrounding earthquakes hereinafter, which includes 3 mainshocks with $5.5 \leq M_L \leq 6.0$ and 25 aftershocks with $M_L \geq 5.5$.

Active fault systems also play a vital role in the process of earthquake nucleation and propagation considering stress transfer. In central Taiwan, there are several important active fault systems identified through geomorphic and field investigations, augmented by modern geodetic and seismological data (Shyu et al., 2016). The main fault systems in order from north to south are as follows: CLPF, Shungtung fault (STF), Changhua fault (CHF), flat decollement of central Taiwan (FDCT), Chukou fault (CKF), Hsinhua fault (HHF), Chishan fault (CSF), and Chaochou fault (CCF) (outlined and marked in Figure 1), respectively. The CHF is a blind thrust fault and about 80 km long. It is a north to south trending fault located in the front of the western foothill belt and was ruptured by a damaging earthquake (~M 7.1) in 1856 (Wang et al., 2003). The CLPF is one of the most known reverse faults in Taiwan, which was ruptured by the 1999 Chi-Chi earthquake causing tremendous life and financial losses. The rupture characteristics of the 1999 Chi-Chi earthquake inverted from the strong-motion records, GPS data, teleseismic data, and the seismic data indicated that this thrust fault broke along the most active central mountain front (Shyu et al., 2005). The STF is another north to south trending thrust fault located in the east side of the CLPF. As the western Taiwan is an active fold-and-thrust belt, many faults appear to stop at or merge with a shallow-dipping or flat decollement, which is defined as FDCT in our paper (Carena et al., 2002; Suppe, 1976, 1981; Suppe et al., 1987). The CKF is a major bedrock geologic structure, which is located in the southern part of the CLPF. It is a reverse fault with about 30–40° eastward dipping (Hsu et al., 2011). The HHF is a right-lateral, north dipping fault, which was ruptured by the M_L 6.11946 Hsinhua earthquake with variation of dip angles in the subsurface. The CSF is a NE-SW trending reverse fault with significant right-lateral slip component identified from GPS observations (Hsu et al., 2011). The CCF was identified to have both vertical and strike-slip motion from the topographic observations (Shyu et al., 2016).

Table 2
Fault Parameters of Active Faults Used as Receiver Faults for the Second Coulomb Failure Model Analysis

Fault name	Strike (deg)	Dip (deg)	Rake (deg)	Length (km)	Width (km)	Depth (km)	Number of fault patches	Reference
Changhua fault	1–38	30	90	61.7	12	12	45	Shyu et al. (2016)
Shungtung fault	5	30	90	68	6	6	20	Shyu et al. (2016)
Chelungpu fault	Variable 3-D fault geometry (see data repository)						65	Hsu et al. (2009)
Flat decollement of central Taiwan	Variable 3-D fault geometry (see data repository)						94	Hsu et al. (2009)
Chukou fault	30	35	90	40	26	15	32	Hsu et al. (2011)
Chaochou fault	4	75	45	80	16	15	24	Hsu et al. (2011)
Chishan fault	37	50	120	30	20	15	24	Hsu et al. (2011)
Hsinghua fault	250	80	180	10	15	15	1	Hsu et al. (2011)

2.3. Source Faults and Receiver Faults

In this paper, we conducted two different Coulomb failure models based on different choices of the receiver faults. In the first failure model, the receiver faults were designed based on the focal mechanism solutions of the strong mainshocks in the Central-Taiwan-Mainshock earthquake sequence (Table 1), whereas in the second model, specific active fault systems (Table 2) were set as the receiver faults. In both study types, source faults were selected from the list of Central-Taiwan-Mainshock sequence and from the list of surrounding earthquakes (Table S1 in the supporting information).

In the first Coulomb stress analysis model, we calculated the cumulative Coulomb stress changes due to large earthquakes in the Central-Taiwan-Mainshock sequence and surrounding earthquakes including smaller magnitude mainshocks and aftershocks. We first chose each earthquake from the Central-Taiwan-Mainshock sequence as a receiver fault and its preceding earthquakes in the same sequence as source faults to explore earthquake interaction effects among the earthquake sequence. For designing the source faults, the fault slip parameters of the 1906 Meishan, 1935 Hsinchu, 1941 Chungpu, 1998 Rueyli, and 1999 Chi-Chi earthquakes were selected from published studies. The slip model of the 1906 Meishan earthquake was resolved from historical seismic records (Liao et al., 2018). The source slip models of the 1935 Hsinchu and 1941 Chungpu earthquakes were generated through geodetic data and earthquake focal mechanism solution, respectively (Lin et al., 2013; Lin & Xiao, 2004). The slip model of the 1998 Rueyli earthquake was determined by near-source strong-motion waveforms (Ma & Wu, 2001). The slip model of the 1999 Chi-Chi earthquake proposed by Hsu et al. (2009) was used, because it includes a complex fault geometry that matches well with the observed fault surface rupture trace and this model fits to the geodetic data better than the models in previous studies (Chi et al., 2001; Johnson et al., 2001; Ma et al., 2000, 2001; Zhang et al., 2004). For all other source faults, slip models were estimated using the empirical relationships of Wells and Coppersmith (1994) based on the focal mechanism information obtained from the TEC compiled by the CWBSN, global CMT catalog, and other resources listed in Table S1. For receiver faults, we use some of the source parameters of the fault planes based on the focal mechanism information of those mainshocks summarized in Table 1.

As suggested by Wang et al. (2017), the influences of surrounding large earthquakes on altering the amounts of Coulomb failure stress changes at each hypocenter of their targeted cannot be ignored. Thus, we also calculated the Coulomb stress changes due to surrounding earthquakes at each hypocenter of the abovementioned earthquakes in the sequence of the first model. For designing the source faults, we selected the earthquakes with $M_L >= 5.5$ from 1900 to 2017 obtained from the CWBSN, which include 28 events (blue dots in Figure 1b and Table S1). The receiver faults are designed based on the focal mechanism information of large mainshocks in the Central-Taiwan-Mainshock sequence in Table 1.

In the second Coulomb failure model, we calculated the Coulomb stress changes on several active faults in central Taiwan to evaluate whether these preceding earthquakes have altered the stress states significantly, which promote or delay the rupture propagation of earthquakes in the sequence or the occurrence of large earthquakes in the future. We designed the source faults in this model based on all preceding earthquakes with $M_L >= 5.5$, which includes not only the mainshocks from the sequence but also the surrounding large earthquakes (Table S1). For the receiver faults, we used the abovementioned eight active faults with published fault parameters (Hsu et al., 2011; Shyu et al., 2016) of near earthquakes in the Central-Taiwan-Mainshock sequence (Table 2). The FDCT is designed based on the 3-D fault geometry constrained by surface geology and seismic profiles, which is the same source for the CLPF (Hsu et al., 2009; Yue et al., 2005). Receiver fault structures of the other active faults are simply generated based on the fault parameters listed in Table 2. The 3-D fault geometry of the CHF includes strong variation of fault strike angle (1° to 38°) from north to south considering the surface trace (Shyu et al., 2016).

3. Results

We first present the cumulative ΔCFS at hypocenters of mainshocks in the Central-Taiwan-Mainshock earthquake sequence due to all preceding earthquakes including both large mainshocks in the Central-Taiwan-Mainshock sequence and surrounding earthquakes (section 3.1). We then present the calculated ΔCFS on the specified active faults in central Taiwan due to all preceding events before the occurrence of each mainshock (section 3.2).

3.1. Coulomb Stress Change at Hypocenters of Mainshocks

We calculated ΔCFS at the hypocenter of each targeted mainshock to quantitatively investigate coseismic triggering effects on the nucleation of these strong mainshocks. In this section, we present three sets of ΔCFS calculations. First, we present results of ΔCFS calculations due to mainshocks in the sequence only, then ΔCFS results due to surrounding earthquakes only, and lastly, cumulative ΔCFS due to both mainshocks in the sequence and surrounding earthquakes.

In order to calculate ΔCFS due to mainshocks only, we calculated ΔCFS for each mainshock in the sequence (Table 1), assigning each mainshock in the sequence as receiver fault and all previous mainshocks in the same sequence as source faults. Since there is no information of mainshocks with $M_L \geq 6.0$ occurring before 1906, we could not estimate stress transfer at the hypocenter of the 1906 Meishan earthquake. Thus, the first mainshock is used only as source fault. We present the calculated results on the receiver faults due to each source fault slip as well as the cumulative ΔCFS due to all preceding source faults (Table S2). We also included information on the magnitudes of the mainshocks used as source faults, as the calculated ΔCFS are strongly dependent on this parameter.

The cumulative ΔCFS for all targeted mainshocks range from −15.82 to 12.21 bars (Table S2). The 1935 Hsinchu, 1941 Chungpu, and 1946 Hsinhua earthquakes were all primarily influenced by the 1906 Meishan earthquake. The 1964 Baihe, 1998 Rueyli, 1999 Chi-Chi, and 2010 Jiashian earthquakes were mostly affected by the 1941 Chungpu earthquake as 5.81 bars, −13.63 bars, 0.41 bar, and 0.24 bar, respectively. The 1972 Hualien and 1983 Taipingshan earthquakes received the largest ΔCFS, approximately 0.51 and 0.34 bar, respectively, from the 1935 Hsinchu earthquake. The 2009 Nantou earthquake received significant ΔCFS induced by the 1906 Meishan, 1935 Hsinchu, 1941 Chungpu, and 1999 Chi-Chi earthquakes. The March 2013 Nantou earthquake received the largest positive ΔCFS (~11.85 bars) from the 1999 Chi-Chi earthquake and also significant ΔCFS (0.33 bar) from the 1935 Hsinchu earthquake of secondary importance. The June 2013 Nantou earthquake was mostly affected by the 2013 March Nantou earthquake and the 1999 Chi-Chi earthquake, which happened in the nearby region. The 2016 Meinong earthquake received significant ΔCFS from the 1906 Meishan, 1935 Hsinchu, 1941 Chungpu, 1946 Hsinhua, and 2010 Jiashian earthquakes. In summary, coseismic rupture during the 1906 Meishan, 1935 Hsinchu, 1941 Chungpu, and 1946 Hsinhua earthquakes had great influence on the occurrence of subsequent large mainshocks at least after 70 years, with longest stress effect identified for even 110 years. The destructive rupture during the 1999 Chi-Chi earthquake played a significant role in promoting or inhibiting the mainshocks in the following 15 years.

Spatial patterns of the cumulative ΔCFS for all the 13 large mainshocks listed in Table 1 are presented in Figure 2. For 8 out of 13 mainshocks, ΔCFS at the hypocenters of those targeted mainshocks were greater than 0.1 bar (Figures 2d–2f, 2h, and 2j–2m marked by red thick frames), indicating that the 8 large mainshocks were significantly promoted to failure by preceding large earthquakes in the same mainshock sequence, whereas ΔCFS at the hypocenters of the remaining 5 mainshocks were smaller than −0.1 bar (Figures 2a–2c, 2g, and 2i with blue thick frames), indicating that 5 large mainshocks were significantly

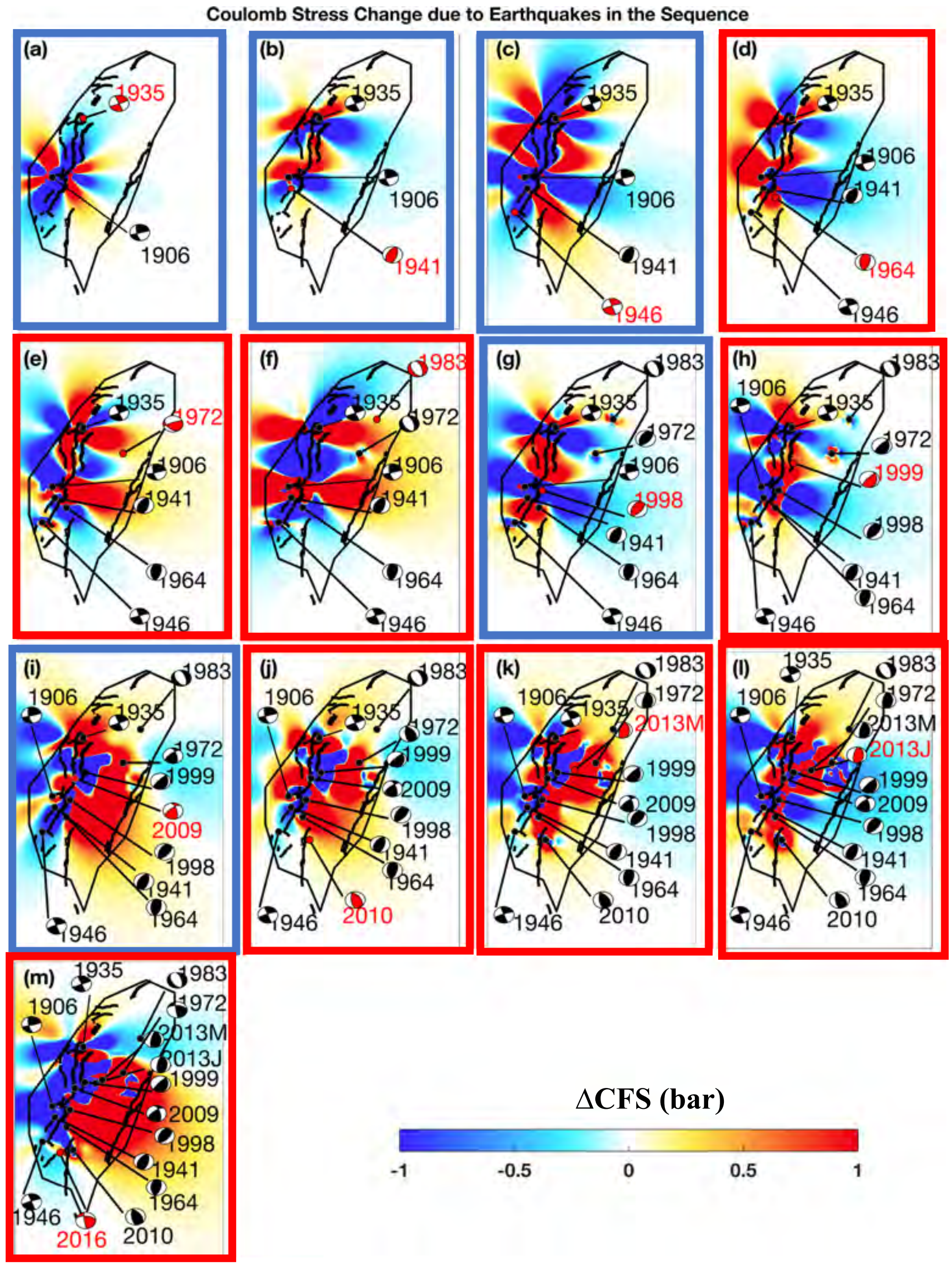

Figure 2. (a–m) Cumulative ΔCFS from preceding mainshocks in the Central-Taiwan-Mainshock sequence at hypocenters of subsequent mainshocks. In each subplot, the red beach ball represents the mainshock, which is the receiver fault, and black beach balls represent the preceding mainshocks in the same sequence set as the source faults. Blue and red thick frames indicate $\Delta CFS \le -0.1$ bar and $\Delta CFS \ge 0.1$ bar at the hypocenter of each mainshock, respectively. The color scale of ΔCFS is chosen between −1 and 1 bar to reflect the significant variation of ΔCFS.

inhibited to failure by the occurrence of their preceding large mainshocks in the Central-Taiwan-Mainshock earthquake sequence.

Next, we investigate coseismic stress triggering effects on the mainshocks from surrounding earthquakes, which include 3 mainshocks with $5.5 \le M_L \le 6.0$ and 25 aftershocks with $M_L \ge 5.5$ occurring from 1900 to 2017. This investigation is crucial, because large surrounding earthquakes could also modify the stress

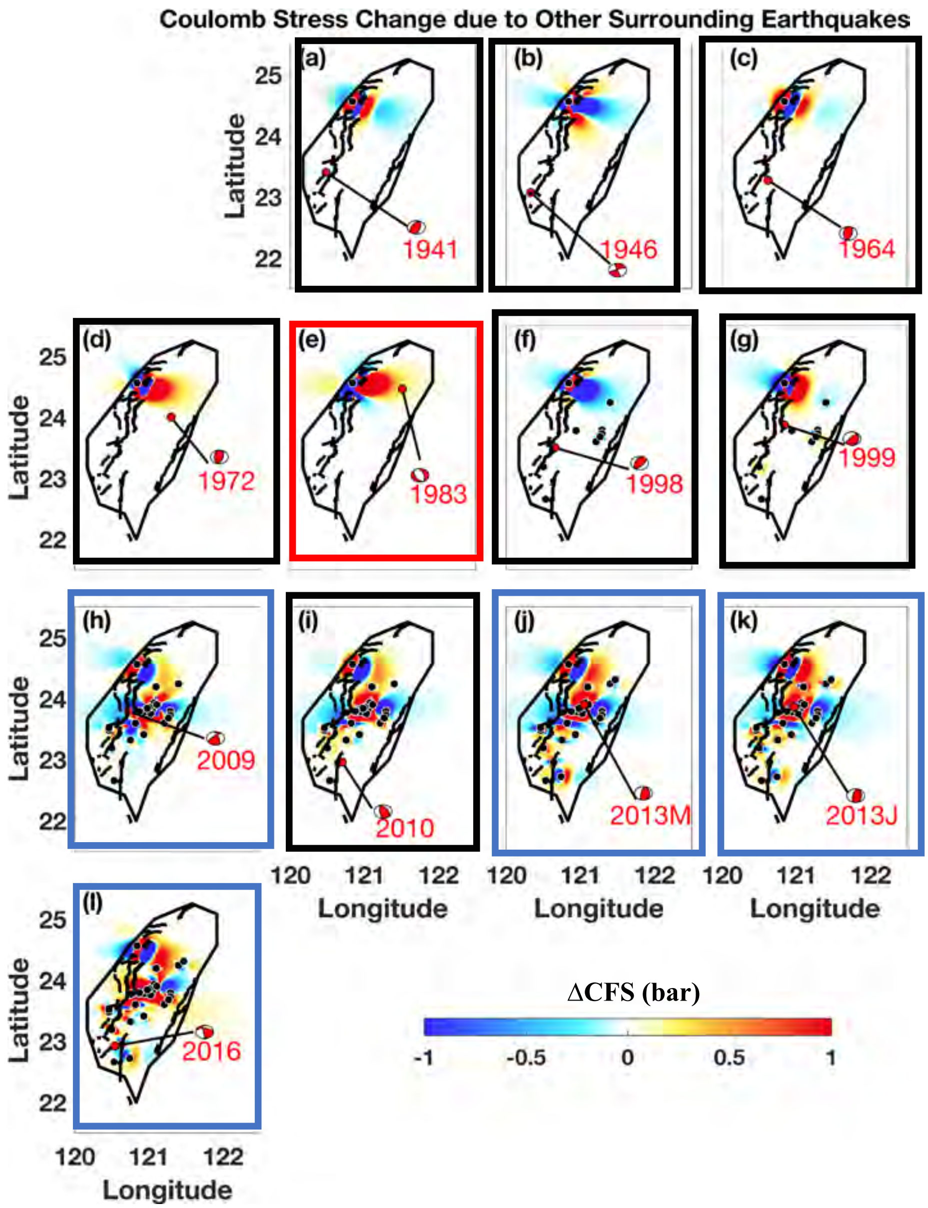

Figure 3. (a–l) Cumulative ΔCFS induced by surrounding earthquakes at hypocenters. In each subplot, red beach balls represent the mainshocks that are receiver faults. Black dots represent the surrounding earthquakes that were considered as source faults. Blue, red, and black thick frames indicate $\Delta CFS \leq -0.1$ bar, $\Delta CFS \geq 0.1$ bar, and $-0.1 < \Delta CFS < 0.1$ bar at the hypocenter of each mainshock, respectively. The color scale of ΔCFS is chosen between −1 and 1 bar to reflect the significant variation of ΔCFS.

states at each hypocenter. Figure 3 shows the resolved ΔCFS due to surrounding earthquakes on the receiver fault plane of each subsequent mainshock. Based on the earthquake history in central Taiwan, there were no records for earthquakes with $M_L \geq 5.5$ before 1935. Therefore, no stress triggering effects from surrounding earthquakes at hypocenters of the 1906 Meishan and 1935 Hsinchu earthquakes were calculated. The hypocenters of four mainshocks (Figures 3h and 3j–3l with blue thick frames) of the earthquake sequence have negative ΔCFS, which suggests that those earthquakes were inhibited to some extent. Those events include the 2009 Nantou, 2013 Nantou in March, 2013 Nantou in June, and 2016 Meinong earthquakes, which were also significantly affected by the strong mainshocks in the sequence (Figures 2i and 2k–2m). In one case, the 1983 Taipingshan earthquake, ΔCFS at the hypocenter of this mainshock was greater than 0.1 bar

Table 3
Cumulative ΔCFS (unitUnit: bar) at the hypocenter Hypocenter of each Each targeted Targeted mainshock Mainshock Due to Preceding Mainshocks With $M_L \geq 6.0$ and Surrounding Earthquakes With 3 mainshocks With $5.5 \leq M_L \leq 6.0$ and 25 Aftershocks With $M_L \geq 5.5$

Receiver fault	Source fault		
Mainshocks	Mainshocks	Surrounding earthquakes	Total
1906/3/16	—	—	—
1935/4/20	−0.21	—	−0.21
1941/12/16	−0.28	0	−0.28
1946/12/4	−1.07	0	−1.07
1964/1/18	5.93	0	5.93
1972/11/9	0.35	0.03	0.38
1983/5/11	0.26	0.27	0.53
1998/7/17	−15.82	0.01	−15.81
1999/9/20	0.72	0.02	0.74
2009/11/5	−0.55	−0.71	−1.26
2010/3/4	0.29	−0.01	0.28
2013/3/27	12.21	−16.92	−4.71
2013/6/2	4.08	−42.57	−38.49
2016/2/5	0.21	−0.11	0.10

Note. Date format is yyyy/mm/dd.

(Figure 3e), which suggested that this mainshock was significantly promoted by the surrounding earthquakes. For the remaining seven mainshocks, ΔCFS at their hypocenters all indicated negligible effect from their preceding surrounding earthquakes (Figures 3a–3d, 3f, 3g, and 3i marked by black thick frames).

In order to evaluate the cumulative ΔCFS at all hypocenters of the mainshocks, we combined the stress triggering effects induced by all preceding earthquakes, including mainshocks in the sequence and surrounding earthquakes from the above two analyses (Table 3). The combined ΔCFS values reveal that the values of the ΔCFS at hypocenters of the two Nantou mainshocks in 2013 changed from positive to negative because the surrounding earthquakes have modified the stress states at hypocenters of these two mainshocks. In addition, we found noticeable changes in the magnitude of the ΔCFS at hypocenters of the 1983 Taipingshan, 2009 Nantou, and 2016 Meinong earthquakes. In summary, 5 of 13 mainshocks were significantly promoted (1964 Baihe, 1972 Hualien, 1983 Taipingshan, 1999 Chi-Chi, and 2010 Jiashian earthquakes), 1 event was potentially promoted (2016 Meinong), as ΔCFS at its hypocenter was 0.10 bar, which is the triggering threshold, and 7 events were inhibited to failure (Table 3). Comparing Figures 2 and 4 shows that the spatial patterns of the ΔCFS become more heterogeneous when considering both mainshocks and surrounding earthquakes. These significant differences indicate that the ΔCFS from surrounding earthquakes resulted in quite different values of ΔCFS than those from the Central-Taiwan-Mainshock earthquake sequence with a few earthquakes.

3.2. Coulomb Stress Change on Nearby Active Fault Systems

In this section, we investigate the influence of all preceding earthquakes including large mainshocks and surrounding earthquakes on nearby fault systems. We computed the ΔCFS on active faults (Table 2) in central Taiwan before the occurrence of each mainshock in the sequence. As mentioned in section 2.2, all the preceding earthquakes with $M_L \geq 5.5$ were regarded as source faults, and receiver faults were active faults defined in Table 2. Through this analysis, we aim to explore how previous earthquakes modified the nearby fault stress field, especially the ones which were located close to the subsequent mainshocks in the sequence. In addition, we calculated ΔCFS on rupture planes of subsequent mainshocks due to preceding earthquakes before the occurrence of each major mainshock in the sequence. Whether preceding earthquakes promoted the rupture propagation of each subsequent mainshock or not is explored. For this analysis, all the preceding earthquakes with $M_L \geq 5.5$ before each subsequent mainshock were regarded as source faults, and receiver faults were rupture plane of each mainshock designed based on source slip distribution model for each major mainshock in Table S1.

We computed ΔCFS on all eight active faults (Table 2) and rupture planes of all subsequent mainshocks induced by preceding earthquakes before each mainshock in the Central-Taiwan-Mainshock sequence. As shown before, lack of information prior to 1906 does not allow us to estimate ΔCFS before the 1906 Meishan event. Prior to the occurrence of the 1935 Hsinchu mainshock, we considered only the contributions from the 1906 Meishan mainshock as the source fault. This calculation indicates significant positive ΔCFS in the southern parts of the CHF (~0.3 bar) and CLPF (0.2 to 0.6 bar), most STF (0.2 to 0.6 bar) and CKF (0.2 to 1 bar), and northern part of CCF (~0.2 bar). The occurrence of the 1906 Meishan mainshock also imposes significant positive ΔCFS in a range of 0.6 bar to 6 bars on both northern and southern end of the 1941 Chungpu rupture plane and ΔCFS in a range of 0.3 bar to 10 bars on northern part of the 1998 Rueyli earthquake rupture plane (Figure 5a).

We continue our study by adding the ΔCFS contribution of all earthquakes preceding a mainshock of the Central-Taiwan-Mainshock sequence to the eight active faults and rupture planes of subsequent mainshocks. Due to limited space, the figures presenting this sequence are provided in the support information (Figure S1). Prior to the occurrence of the 1941 Chungpu mainshock, coseismic ruptures of the 1935 M_L

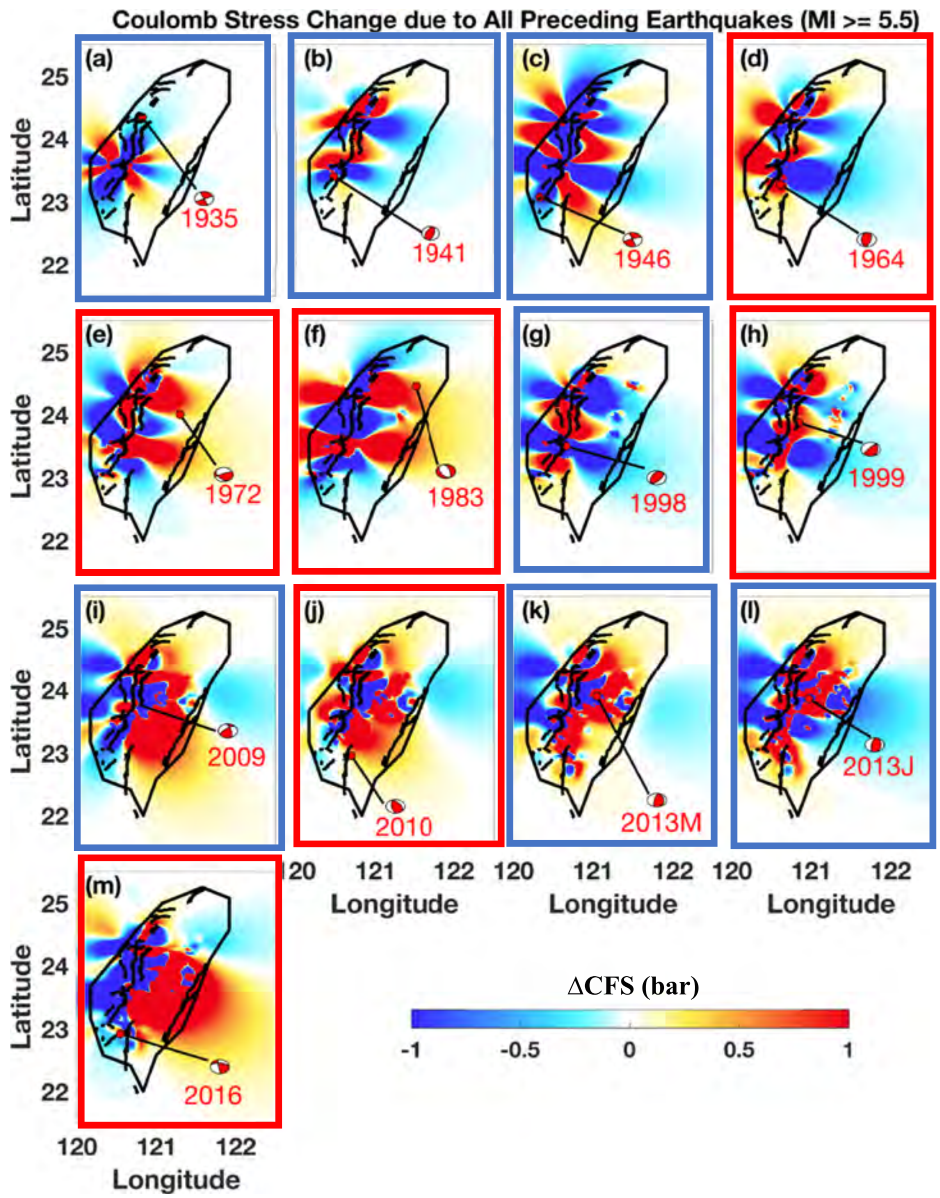

Figure 4. (a–m) The cumulative ΔCFS induced by all preceding earthquakes including mainshocks in the Central-Taiwan-Mainshock sequence and surrounding earthquakes at hypocenters. In each subplot, red beach balls represent the mainshock that was used as receiver faults. Blue, red, and black thick frames indicate ΔCFS ≤ −0.1 bar, ΔCFS ≥ 0.1 bar, and −0.1 < ΔCFS < 0.1 bar at the hypocenter of each mainshock, respectively. The color scale of ΔCFS is chosen between −1 and 1 bar to reflect the significant variation of ΔCFS.

7.3 Hsinchu mainshock and M_L 6.8 aftershock resulted in significant positive ΔCFS in a range of 2 to 15 bars on the central portion of CHF and ΔCFS in a range of 1 to 3 bars on the FDCT (Figure S1a). Prior to the occurrence of the 1946 Hsinhua earthquake, 1941 Chungpu mainshock imposed significant positive ΔCFS in a range of 0.1 to 0.3 bar on most of the CSF and up to 10 bars near the downdip end (depth is larger than 10.5 km) of the 1998 Rueyli earthquake rupture plane (Figure S1b). After 5, 18, 26, and 37 years, the occurrence of the 1946 Hsinhua, 1964 Baihe, 1972 Hualien, and 1983 Taipingshan earthquakes, respectively, did not change the stress field on active faults and rupture planes of subsequent mainshocks significantly comparing from Figures S1b to S1f. Then before the 1999 Chi-Chi earthquake struck, the occurrence of the 1998 Rueyli earthquake and some other smaller events with $M_L \geq 5.5$ did not change significantly the stress field along nearby fault systems and rupture planes of mainshocks significantly

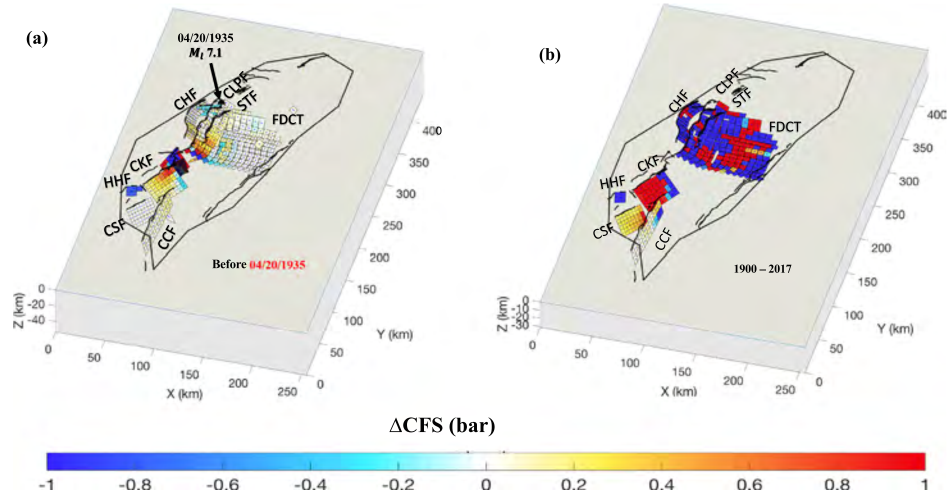

Figure 5. (a) Calculated ΔCFS on the seven predefined active faults (Table 2) induced by the coseismic ruptures of preceding earthquakes before the 1935 Hsinchu mainshock occurred. The black dot where a black arrow points to represents the epicenter of subsequent mainshock in the analysis. (b) Cumulative ΔCFS on specified active faults induced by all preceding earthquakes from 1900 to 2017. CHF: Changhua fault; CLPF: Chelungpu fault; STF: Shungtung fault; FDCT: flat decollement of central Taiwan; CKF: Chukou fault; HHF: Hsinghua fault; CCF: Chaochou fault; CSF: Chishan fault. The color scale of ΔCFS is chosen between −1 and 1 bar to reflect the significant variation of ΔCFS.

(Figures S1f and S1g). Within the decade before the 2009 Nantou earthquake happened, the sequential ruptures of the 1999 Chi-Chi earthquake, its aftershocks, and some other smaller events with $M_L \geq 5.5$ imposed significant positive ΔCFS for about 0.2 bar at the CSF and CCF, up to 25 bars in the middle part of flat decollement, and significant negative ΔCFS on the CHF, STF, and most shallow portion of the CLPF (Figure S1h). Later, before the occurrence of the 2010 Jiashian earthquake, the coseismic slip from the 2009 Nantou mainshock and its aftershock did not change significantly the stress field on nearby faults significantly (Figure S1i). After about 5 months, before the occurrence of the 2013 Nantou mainshock in March, the accumulative stress triggering effects from the 2010 Jiashian mainshock and another two large earthquakes modified the stress field on the CCF with smaller ΔCFS comparing with Figure S1i and imposed ~2 bars ΔCFS in the northern end of the CSF (Figure S1j). Lastly, before the occurrence of the June 2013 Nantou mainshock and 2016 Meinong earthquake, the coseismic ruptures of the two 2013 Nantou mainshocks did not change the stress field in surrounding fault region significantly (Figures S1k and S1l).

Furthermore, we considered all the existing earthquakes with $M_L \geq 5.5$ from 1900 to 2017 including both mainshocks in the sequence and surrounding earthquakes as the source faults and then the active faults as receiver faults. The results in this analysis reveals that significant positive ΔCFS have been observed on the CKF (~5 bars), CSF (~2 bars), northern side of CCF (~2 bars), and FDCT (2–35 bars) (Figure 5b). Snapshot of ΔCFS on each major active fault due to preceding earthquakes from 1900 to 2017 is included in the supporting information (Figure S2).

4. Sensitivity Studies

The Coulomb failure model involves computing shear and normal stress changes on a receiver fault caused by changes of the stress field due to source fault slip. However, ΔCFS results were calculated without consideration of uncertainties. In order to investigate ΔCFS uncertainties due to uncertainties in the source and receiver fault locations, geometries, and slip distribution, we conduct sensitivity studies, in which we vary some of the main parameters within a reasonable range. In the following several subsections, we investigate the variability of the calculated ΔCFS at hypocenters of two mainshocks due to the uncertainties in source slip models, receiver fault parameters, location of hypocenters, and the effective friction coefficient. One of the selected mainshocks is located close to the source fault (within 21 km), which means that the receiver fault is located in the near field of the source fault, whereas the other is located farther away

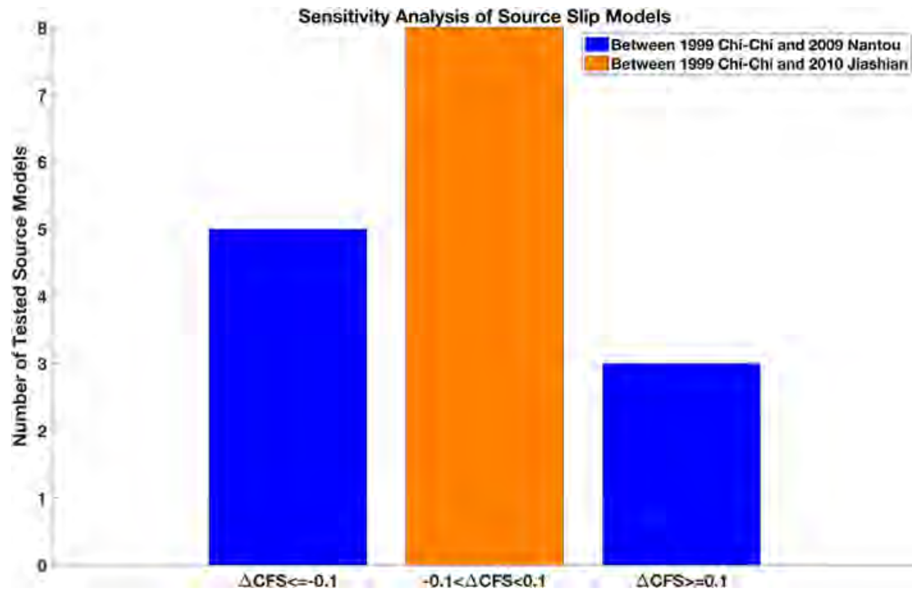

Figure 6. Sensitivity of ΔCFS at hypocenters of the 2009 Nantou (blue bars) and 2010 Jiashian mainshocks (orange bars) due to different source slip models of the 1999 Chi-Chi earthquake shown in the histogram. Histogram show distribution of calculated ΔCFSs in three bins: $\Delta CFS \geq 0.1$ bar, $\Delta CFS \leq -0.1$ bar and $-0.1 < \Delta CFS < 0.1$ bar.

from the source fault (> 100 km), which means that the receiver fault is located in the far field of the source fault.

In all the sensitivity studies, we evaluate the sensitivity of ΔCFSs at hypocenters of subsequent mainshocks, by using two examples of the 1999 Chi-Chi earthquake as source fault and the 2009 Nantou and 2010 Jiashian events as receiver faults. We chose Chi-Chi earthquake as source fault because it was the only mainshock that has several available source slip models. We chose the 2009 Nantou earthquake as receiver fault because this mainshock is one of the large earthquakes in the sequence that is significantly affected from the coseismic striking of the 1999 Chi-Chi mainshock. We chose the 2010 Jiashian event as another receiver fault because this event is one of the subsequent mainshocks located farther away from the source fault, which allows us to test the sensitivity of the model for such a distant case.

4.1. Sensitivity of Coulomb Stress Change Caused by Different Source Slip Models

Multiple finite source models of the 1999 Chi-Chi earthquake have been generated using various geometries and constraining data types (Chi et al., 2001; Duan & Oglesby, 2006; Hsu et al., 2009; Johnson et al., 2001; Ma et al., 2000, 2001; Mai & Thingbaijam, 2014; Zhang et al., 2004). In general, all the published fault slip models show common features: (1) coseismic slip during the Chi-Chi earthquake ruptured the north to south trending CLPF for a length of about 100 km, (2) large coseismic displacements occurred in the northern portion of the CLPF, and (3) reverse faulting was dominant along most of the north to south rupture. However, these slip distributions are quite different in details among the models, which were generated using different inversion techniques, different model parameterizations, and different data. The models differ from one another by (1) spatial pattern of slip magnitude, especially the calculated peak slip magnitude and its spatial coverage; (2) fault geometry; some slip models are simple planar model, whereas other models include more complex surface rupture patterns; and (3) source parameters including the location of hypocenter, the strike, dip, rake angle, and length and width of the ruptured fault.

Table 4
Calculated ΔCFS at the Hypocenter of the 2009 Nantou and 2010 Jiashian Events Due to Different Source Slip Models of the 1999 Chi-Chi Earthquake

Source slip models	ΔCFS_{2009} (bar)	ΔCFS_{2010} (bar)	Reference
1999Yaru	−0.72	0.06	Hsu et al. (2009)
1999Chie	2.79	0.06	Chi et al. (2001)
1999CMT	26.09	0.09	Global CMT Catalog
1999John	−1.56	0.06	Johnson et al. (2001)
1999Ma00	−5.52	0.03	Ma et al. (2000)
1999Ma01	5.10	0.04	Ma et al. (2001)
1999Seki	−1.05	0.02	Zhang et al. (2004)
1999USGS	−3.31	0.05	USGS finite source model

The sensitivity analysis of the eight fault slip models indicates small ΔCFS variation in the far field (Figures 6 and S3i–S3p) and large variation in the near field (Table 4 and Figures 6 and

S3a–S3h). In general, a simple planar model presents the main features of the ΔCFS in the far field, which is the same as using a more complicate slip model. But a more complicated source slip model makes the ΔCFS distribution heterogenous in the near field on the receiver fault. In summary, the source slip models have a strong influence on the ΔCFS distribution on the receiver fault in the near field (Figures 6 and S3a–S3h) and minor effect on the ΔCFS on the receiver fault in the far field (Figures 6 and S3i–S3p). Therefore, a more detailed earthquake slip model is better for the ΔCFS calculation, especially when the receiver fault is within near field of the source fault.

The sensitivity analysis between the 1999 Chi-Chi and 2009 Nantou earthquakes indicates large variation in the calculated ΔCFS based on different source slip models (Figure 6). However, only one model yields very high value of ΔCFS (>25 bars), which can be considered as an outlier. All other seven models yielded values in the range of −5 to +5 bars, and three of the seven are with value in the range −2 bars to −0.5 bar (Table 4). The mean and standard deviation of the seven models are −0.61 bar and 3.5 bars, whereas sensitivity analysis between the 1999 Chi-Chi and 2010 Jiashian earthquakes suggests negligible variation in the calculated ΔCFS, and all values fall within the range between −0.1 and 0.1 bar, which is considered as no significant stress change.

For the main study exploring the Coulomb stress triggering effects due to preceding earthquakes on the rupture process of subsequent mainshocks, we chose the source slip model of the 1999 Chi-Chi earthquake proposed by Hsu et al. (2009), because (1) this coseismic slip model used the 3-D fault geometry proposed by Yue et al. (2005), which is well constrained by the local surface geology and reliable seismic profiles and matches well with the fault surface rupture trace during the this large earthquake; (2) it fits the surface observation with a smaller root mean square misfit (wrms) than other models; (3) it is based on a heterogenous slip pattern from surface to depth, which matches well with the local structural geology constraints.

4.2. Sensitivity of Coulomb Stress Changes Caused by Receiver Fault Geometry (Strike, Dip, and Rake)

Previous studies suggest that the static Coulomb stress transfer can be sensitive to changes in strike, dip, and rake angles of the receiver faults in different tectonic regions (Mildon et al., 2016; Wang et al., 2014). To analyze the impact of receiver fault geometry on the calculated ΔCFS, we systematically vary the strike, dip, and rake values of the receiver fault and compare their influence on the calculated ΔCFS at hypocenters of the mainshock. As before, we used the source slip model of the 1999 Chi-Chi earthquake proposed by Hsu et al. (2009) as source fault and the 2009 Nantou and 2010 Jiashian earthquakes as receiver faults for two pairs of sensitivity analysis on receiver fault geometry. The original receiver fault geometry is 230°/59°/139° (strike/dip/rake) for the 2009 Nantou mainshock based on global CMT catalog and 324°/39°/67° for the 2010 Jiashian mainshock (Hsu et al., 2011). We varied the strike, dip, and rake angle of the receiver fault within a range of 10°, respectively, and calculated the new ΔCFS at hypocenters of the 2009 Nantou and 2010 Jiashian mainshocks. We limited the analysis to ±10°, because this variation range for each parameter should be large enough to cover the potential uncertainty, which was less than 7°, in the strike, dip, and rake angles of receiver fault in reality (Wu, Zhao, et al., 2008).

For the sensitivity analysis between the 1999 Chi-Chi and 2009 Nantou earthquakes, which is located close to source Chi-Chi event, for a strike angle increases from 220° to 240°, the calculated ΔCFS at hypocenter also increases. There was only a magnitude change in the ΔCFS, and all calculated values remained negative and smaller than −0.1 bar. The stresses are located in the range of −1.34 bars to −0.22 bar, with mean and standard deviation as −0.74 and 0.35 bar (Figure S4a). Opposite to the sensitivity results of the strike angle, the calculated ΔCFS at the hypocenter increases when the dip angle increases from 49° to 69°. Most calculated values remained negative and smaller than −0.1 bar, except that ΔCFSs of two models with dip angle of 68° and 69° are slightly larger than −0.1 bar and, hence, can be regarded as outliers. All calculated values are located in the range of −1.61 bars to −0.03 bar, with mean and standard deviation as −0.76 and 0.49 bar (Figure S4b). Similarly, when varying the rake angle, the calculated ΔCFS at the hypocenter decreases when the rake angle increases from 129° to 149°. All calculated values remained negative and smaller than −0.1 bar. They are all located in the range of −1.02 bars to −0.43 bar, with mean and standard deviation as −0.72 and 0.18 bar (Figure S4c).

For the sensitivity analysis between the 1999 Chi-Chi and 2010 Jiashian earthquakes, which is located far away from the source Chi-Chi event, calculated ΔCFS at hypocenter slightly increases as strike angle increases from 314° to 334° and dip angle increases from 29° to 49°, whereas calculated ΔCFS at hypocenter slightly decreases as rake angle increases from 57° to 77°. Almost all calculated values for variation of three parameters are located within the range of −0.1 to 0.1 bar, which are regarded as negligible stress change (Figures S4d–S4f), with one exception that ΔCFS is exactly 0.1 bar with dip angle of 49° thus can be considered as an outlier. In summary, the sensitivity tests on the receiver fault geometry reveal that calculated ΔCFS at a hypocenter of a mainshock can be quite sensitive to the assumed geometry (strike, dip, and rake) of the receiving fault, but only in receiver faults that are located in near field. The calculated changes in ΔCFS are mainly in the magnitude with no polarity changes when receiver faults are located in the far field.

4.3. Sensitivity of Coulomb Stress Changes Caused by Location of Mainshocks (Longitude, Latitude, and Focal Depth)

The uncertainty in the location of hypocenters of the mainshocks can potentially affect the accuracy of the calculated ΔCFS at hypocenters. In order to explore the impact of mainshock location on the calculated ΔCFS, we conducted two analyses: one is varying the horizontal location of epicenter including longitude and latitude and fixing the focal depth and the second one is only varying the focal depth with fixed epicenter. As before, we used the 2009 Nantou and 2010 Jiashian events as receiver faults and the 1999 Chi-Chi earthquake as source fault. The initial location of hypocenters for the 2009 Nantou and 2010 Jiashian mainshocks are shown in Table 1.

We varied the location of epicenter of the 2009 Nantou mainshock within a 0.2° × 0.2° (roughly 20 × 20 km) range (black box in Figure S5a) with the initial location in the center through changing interval in longitude and latitude by 0.01° and keeping the focal depth fixed. We chose the variation of location of epicenter in a 0.2° × 0.2° range because this range should be large enough to cover the potential uncertainty, which was less than 10 km, in the location of epicenter of the mainshock when using local network data (Wu, Chang, et al., 2008). The sensitivity analysis on the location of epicenter reveals that there was only magnitude change in the ΔCFS at the hypocenter if the location error of the epicenter is smaller than 2 km in all directions. When the location error of the epicenter is larger than 2 km, the calculated ΔCFSs indicate changes in both magnitude and polarity (Figure S5a). We also explored solution sensitivity to focal depth, by varying the depth within a range of ±5 km with interval of 0.1 km. We found that the calculated ΔCFS at hypocenter decreases when the focal depth increases from 19.08 to 29.08 km. Obvious changes in magnitude and polarity of the ΔCFS have been found when the focal depth was shallower than 20.88 km. The ΔCFS remained significantly negative with magnitude change only when the focal depth is deeper than 21.68 km. All calculated ΔCFSs are located in the range of −1.66 bars to 0.58 bar, which spanned three bins: $\Delta CFS \geq 0.1$ bar, $\Delta CFS \leq -0.1$ bar and $-0.1 < \Delta CFS < 0.1$ bar, with mean and standard deviation as −0.65 and 0.68 bar (Figure S5b).

We used the same above method above to conduct the sensitivity analysis of hypocenter location using the 1999 Chi-Chi earthquake as source fault and the 2010 Jiashian earthquake as receiver fault. The analysis indicates that minor changes in calculated ΔCFS have been found no matter how we varied the location of epicenter (longitude and latitude) or the focal depth. All the calculated values locate within one bin, which is $-0.1 < \Delta CFS < 0.1$ bar (Figures S5c–S5d). In summary, the calculated ΔCFS is sensitive to the uncertainty in the hypocenter location of the mainshock when receiver fault is in near field of source fault but not sensitive at all when receiver fault is in the far field. The sensitivity analysis in this section indicates the significance in obtaining more detailed information about uncertainty in mainshocks location in the future Coulomb failure analysis.

4.4. Sensitivity of Coulomb Stress Changes Caused by Effective Friction Coefficient (μ')

The selection of a reasonable value for the μ' is very important because it controls the contribution of the normal stress change in the Coulomb stress calculation (King et al., 1994). Different μ' values should be considered for different fault environments. We set the μ' at 0.4 based on a previous study of earthquake focal mechanisms in Taiwan (Hsu et al., 2011). In this sensitivity study, we varied values of μ' from 0 to 1 with interval 0.1 to analyze their sensitivity on the calculated ΔCFS at hypocenters of the 2009 Nantou and 2010 Jiashian mainshocks. In these calculations, we again used the complex slip model of the 1999

Chi-Chi earthquake proposed by Hsu et al. (2009); fault geometries of receiver faults were designed based on the 2009 Nantou mainshock from CWBSN and the 2010 Jiashian event from Hsu et al. (2011). The sensitivity analysis between the 1999 Chi-Chi and 2009 Nantou events reveals that increasing μ' leads to decreasing ΔCFS at the hypocenter and all values fall in the range of −2.39 bars to 0.39 bar, which spanned two bins: ΔCFS ≥ 0.1 bar and ΔCFS ≤ −0.1 bar. For this sensitivity analysis, most calculated ΔCFSs are smaller than −0.1 bar, except ΔCFSs which are larger than 0.1 bar have been estimated when using the μ' as 0 or 0.1, which can be regarded as outliers (Figures S6a). However, sensitivity analysis between the 1999 Chi-Chi and 2010 Jiashian earthquakes indicates that increasing μ' leads to increasing ΔCFS at the hypocenter. All values fall in the range of 0.01 to 0.14 bar, which spanned two bins: ΔCFS ≥ 0.1 bar and −0.1 < ΔCFS < 0.1 bar in the inset histogram (Figures S6b). Most ΔCFSs are smaller than 0.1 bar and larger than −0.1 bar, except four significant positive ΔCFSs have been estimated when using $\mu' \geq 0.7$.

4.5. Summary of Sensitivity Studies

Our model of Coulomb stress transfer indicates that preceding moderate and large earthquakes from 1900 to 2017 imposed significant stress triggering effects with ΔCFS larger than 0.1 bar or smaller than −0.1 bar on the occurrence of large mainshocks and along active faults in central Taiwan. However, the above sensitivity studies demonstrated that a number of factors could generate uncertainties in the calculated ΔCFS. For the case that receiver fault is close to source fault, first, variation of coseismic slip models of the 1999 Chi-Chi earthquake returns large variation of the calculated ΔCFS at hypocenters of subsequent mainshock. Besides that, the ΔCFS associated with most mainshocks in the Central-Taiwan-Mainshock sequence were calculated using simple slip models. For future work, more reliable calculation will be possible using more accurate variable slip models. Second, comparing among the sensitivity results (especially standard deviations) when varying strike, dip, or rake angle of the receiver faults suggests that the calculated ΔCFSs have larger variation when the dip angle changes while smaller variations are retained when the strike or rake angle varies. Third, change in both magnitude and polarity of the calculated ΔCFS can be sensitive if the error of the location of epicenter is larger than 2 km. We also found that the ΔCFS gets smaller as the focal depth is deeper. While for the case that receiver fault is located farther away from source fault, similar levels of variations have been found for variation of source slip models, strike, dip, and rake angles of receiver fault and hypocenter location. Last, since it was proposed that the friction coefficient is mostly in a range of 0.2–0.5 (Hsu et al., 2010), different option of μ' does not change our conclusion in whether promoting or inhibiting future earthquakes no matter how far receiver fault is located relative to source fault.

5. Discussion

5.1. Earthquake Interactions in Central Taiwan

A principal motive for our investigation of the earthquake interaction effects in central Taiwan was to quantify the impact on nucleation and rupture propagation of large earthquakes from preceding moderate and large events. Coulomb stress analysis at the hypocenters of large mainshocks in the Central-Taiwan-Mainshock sequence has shown that the nucleation of 5 out of 13 mainshocks in the Central-Taiwan-Mainshock earthquake sequence were significantly promoted to failure due to the coseismic rupture of preceding earthquakes with $M_L \geq 5.5$ from 1900 to 2017, while nucleation of 7 mainshocks in the sequence was significantly inhibited. Stress changes at hypocenter of one mainshock, the 2016 Meinong earthquake, did not yield conclusive results, because the calculated ΔCFS at its hypocenter was 0.10 bar, which is the promotion threshold level (0.1 bar). When considering potential uncertainties, the ΔCFS at this event may drop below the threshold level. The uncertainty analysis also reveals that smaller magnitude mainshocks and aftershocks can play a vital role in altering the stress state at hypocenters of large mainshocks.

Coulomb failure models that estimate the stress transfer along nearby active fault systems due to all preceding earthquakes indicate the following: (1) the occurrence of the 1906 Meishan earthquake imposed 0.2 to 0.6 bar ΔCFS near the southern end of the CLPF. Then coseismic rupture of the 1935 Hsinchu earthquakes imposed 1–3 bars ΔCFS on the northern section of the CLPF and flat decollement (Figures 5a and S1a). The region with significant positive ΔCFS matches well with the coseismic rupture trace proposed by Hsu et al. (2009), which are located farther away from the hypocenter and large area of the seismic moment release leading to the striking 1999 Chi-Chi earthquake; (2) coseismic rupture of the 1906 Meishan and 1941 Chungpu earthquakes imposed 0.3 bar to 10 bars and up to 10 bars at the northern section of the

1998 Rueyli rupture plane, which may suggest significant promoting effect on the propagation of the 1998 Rueyli earthquake; (3) coseismic rupture of the 1906 Meishan earthquake imposed up to 6 bars at both northern and southern end of the 1941 Chungpu rupture plane; (4) unless creep or small earthquakes relieves these significant positive stress changes, we can expect to have future nucleation of large earthquakes on the CKF, CSF, CCF, and FDCT. Due to lack of information on how much stress is required for each fault system to accumulate in order to rupture, the significant cumulative ΔCFSs on the central part of the flat decollement, CKF, CSF, and CCF only suggest that these faults may have higher probability to rupture compared to other fault systems but are not able to provide the exact date of next large earthquake.

In conclusion, the occurrences of the moderate and large earthquakes with $M_L \geq 5.5$ over 117 years contribute significantly to the nucleation or rupture propagation of some large earthquakes in central Taiwan, whereas forecasting locations of future earthquakes only based on ΔCFS is not enough, and it requires exploration of other mechanisms or considering a longer historic seismic catalog, which is unavailable now.

5.2. Comparison to Previous Studies

Although some studies of earthquake interaction in central Taiwan examined ΔCFSs from large earthquakes of the Central-Taiwan-Mainshock earthquake sequence (Chan & Stein, 2009; Chan & Wu, 2014; Hsu et al., 2011; Lin et al., 2013; Ma et al., 2005; Mouyen et al., 2010), our paper expanded on these previous studies by considering more surrounding moderate and large earthquakes. There are similarities between our study and previous studies. For instance, the stress interactions indicate that the occurrence of the 1906 Meishan and 1935 Hsinchu earthquakes imposes great influence with significant positive ΔCFS on the nucleation and rupture propagation of the 1999 Chi-Chi earthquake, which agrees well with the findings in Lin et al. (2013). In another example, Mouyen et al. (2010) estimated the effect of both interseismic loading and major events from 1736 to 2006 on the stress state of nearby active fault systems in western Taiwan. They concluded that preceding earthquakes before 1999 on the CLPF induced two patches of Coulomb stress increase located in the northern and southern part of the fault. Our results also confirmed the existence of significant positive ΔCFSs in the northern and southern part of the CLPF with smaller value in the southern part and higher value in the northern part. Our study suggests that the coseismic rupture of the 1999 Chi-Chi earthquake still influence the surrounding stress field after decades and promoted the fault rupture of the two Nantou mainshocks in 2013 to failure, which agrees well with the Chan and Wu (2014) findings. We also found that the 2013 Nantou mainshock in June was significantly promoted by the occurrence of the 2013 Nantou mainshock in March, which agreed well with the conclusion in Liao and Huang (2016).

Yet our study of earthquake interaction in central Taiwan also differs from previous studies by the magnitude or sign of the calculated ΔCFSs at hypocenters of some large earthquakes within the sequence or significant Coulomb stress increasing areas. We attribute the difference to the use of different coseismic slip models for the mainshocks in the earthquake sequence, different number of preceding earthquakes that have been explored, and different fault geometries for the receiver faults. For example, we found a change in magnitude of the calculated ΔCFS at hypocenter of the two Nantou mainshocks in 2013 induced by the 1999 Chi-Chi earthquake when comparing our study and that from Chan and Wu (2014). In addition, our study suggests different magnitude of positive ΔCFS in the northern and southern side of the CLPF from the estimation in Mouyen et al. (2010). They did not find any stress increase existing nearby the initial mainshock location, whereas we identified significant positive ΔCFS at hypocenter of the 1999 Chi-Chi earthquake due to the coseismic slip during the 1935 Hsinchu and 1941 Chungpu earthquakes.

5.3. Comparison to Other Regions

Comparing our results with numerous Coulomb stress studies in other regions suggests multiple similarities in the identified earthquake interaction effects among recent earthquakes as a result of the evolution of the static stress transfer. For example, Syed Tabrez et al. (2008) found that the observed west propagation of the subsequent mainshocks along the strike-slip faults were significantly promoted by the occurrence of preceding large earthquakes with $M_L \geq 7.0$ in the northeastern Caribbean region from 1751 to 2017. In our study, we found significant Coulomb stress increase on the rupture planes of the 1941 Chungpu, 1998 Rueyli, and 1999 Chi-Chi earthquakes, which may also indicate strong influence on rupture propagation of large mainshocks due to preceding earthquakes. In another case, Asayesh et al. (2019) proved that preceding earthquakes for 30 years significantly affected the rupture of the subsequent large mainshocks in the subduction zone between the Arabian and Eurasian plates, of which pattern was also found in our study for central Taiwan through 117-year seismic records. Wang et al. (2017) found that the cumulative ΔCFS at hypocenters of mainshocks happened along the Bayan Har block on the Tibetan Plateau changed when considering additional surrounding earthquakes that were not those targeted mainshocks. Likewise, considering stress effects from surrounding earthquakes also modified the stress state at hypocenters of large mainshocks in central Taiwan with our study.

5.4. Analysis of Sensitivity Results and Comparison to Other Sensitivity Studies

Our sensitivity analysis shows that several parameters including different choices of source slip models, the orientation of the receiver fault (strike/dip/rake), location of mainshock epicenters, mainshock focal depth, and effective friction coefficient may alter the magnitude and/or polarity of the calculated ΔCFS when testing a range of values for each parameter, especially when receiver fault is located in the near field of source fault. In order to evaluate the impact of uncertainties on the calculated ΔCFS at mainshock hypocenters shown in section 3, we conduct a simple statistical analysis about the sensitivity results. For each tested parameter, we assume that a set of calculated ΔCFS values follows the standard normal distribution and calculates the probability for each ΔCFS. It is the simplest assumption that we can make based on the limited available information about large earthquakes. Through multiplying the probability by each ΔCFS, we get a new set of weighted ΔCFS values. Then we recalculate mean and standard deviation for each parameter and get total standard deviation resulted from all tested parameters (Table S3). The simple statistical analysis shows that locations of mainshock epicenter and focal depth play a predominant effect; influences of effective friction coefficient and source slip models cannot be ignored when receiver fault is located close to source fault. The total standard deviation (0.28) considering uncertainties from all parameters (Table S3) is about 38% of the optimal ΔCFS (−0.72) at hypocenter of the 2009 Nantou mainshock due to the 1999 Chi-Chi source slip in Table S2. We used the same statistical analysis method to evaluate the sensitivity analysis between the 1999 Chi-Chi and 2010 Jiashian earthquakes, which is located farther away from the Chi-Chi event. This case study indicates that (1) total standard deviation (0.02 bar) is about 33% of the optimal ΔCFS (0.06 bar) at hypocenter of the 2010 Jiashian mainshock and (2) effective friction coefficient plays a dominant effect when receiver fault is far away from source fault, and other parameters all have minor influence (Table S3). Based on this case study, we propose that around 33–38% of the calculated ΔCFS can be taken into account when analyzing uncertainty derived from earthquake interaction effects in central Taiwan.

A limited amount of Coulomb stress studies has considered or discussed uncertainty in ΔCFS calculations (Catalli & Chan, 2012; Hainzl et al., 2009; Hsu et al., 2011; Wang et al., 2014; Zhan et al., 2011). A comparison between our and the above studies reveal both similarities and differences. Here we discuss couple of points: (1) simplified assumptions in sensitivity analysis and (2) concluded impact of uncertainties on ΔCFS calculations. In our sensitivity study, we assumed no correlation among parameters by estimating each parameter independently with other remaining parameters fixed due to lack of information about possible correlation among parameters. Most previous studies also used the same simple assumption in their sensitivity calculations (Catalli & Chan, 2012; Hainzl et al., 2009; Hsu et al., 2011, Wang et al., 2014; Zhan et al., 2011). The second point we discuss here is the concluded impact of uncertainties on ΔCFS calculations. All the uncertainty studies demonstrated the nonnegligible effect of source slip models, orientation, and focal depth of receiver fault and effective friction coefficient. Our analysis suggests that location of epicenter and focal depth of mainshock are the most sensitive parameters in the calculated ΔCFS. However, Wang et al. (2014) proposed that Coulomb stress changes are most sensitive to the uncertainty in the dip angle of the receiver fault, whereas Catalli and Chan (2012) indicated that focal depth where Coulomb stress was computed was of utmost importance.

5.5. Limitation of Our Study

The first obstacle we had to face in this study is the scarcity of spatial heterogeneity of the coseismic slip models of most earthquakes with $M_L \geq 5.5$ and the geometry of active fault systems. Our findings clearly indicate that the specified source fault and receiver fault mechanism may generate significant uncertainty in the calculated ΔCFS. More reliable slip models or fault geometries can help provide more accurate estimations. Another difficulty is lacking uncertainty information of each important parameter in the Coulomb failure model, as focal depth, epicenter location, receiver fault geometry, and so on. Currently, we can only use information from published results for the different earthquakes. Most of them did not include detailed uncertainty. Third, there are still some controversial ideas about active faults in central and southern Taiwan (e.g., Hsu et al., 2011; Shyu et al., 2016). Especially, the CKF is considered as an active fault in the data set from the Central Geological Survey of Taiwan (Hsu et al., 2011) but is not included in the active structure data of the Taiwan Earthquake Model (Shyu et al., 2016). Based on the field evidences indicating that the fault has not ruptured at least for the past 38,000 years, Shyu et al. (2005) suggested that the fault is not currently active. They also proposed that most of the seismic activity in the area has been shifted farther to the west to the frontal fault systems. However, since the Central Geological Survey data are the official data set in Taiwan, we still use the fault parameters of the CKF to calculate the stress transfer along the CKF due to preceding earthquakes. Even though there are different opinions about the current activity of the CKF (Shyu et al., 2005, 2016), if this fault is still active, then the calculated ΔCFS may promote future earthquake along the fault. Lastly, the positive ΔCFS on a fault does not necessarily mean that the fault will rupture soon, or next. If a fault has ruptured recently, positive ΔCFS from earthquake interactions may not have an immediate impact on the next rupture of this fault. On the other hand, some faults may have ruptured long time ago and are close to rupture again. Even without any positive Coulomb stress changes (or even negative), those faults would still rupture sooner. Therefore, one cannot just use our results to assert which of the active faults may be the next one to rupture.

5.6. Other Earthquake Triggering Mechanisms

Earthquakes are generated mostly in response to stress loading by long-term plate motion. However, it is not the only forcing factor, because otherwise earthquakes will happen in a well-known periodically way. Multiple studies have demonstrated that the rupture of moderate earthquakes can modify the stress state on the nearby fault system, which may promote or inhibit the occurrence of an earthquake (Asayesh et al., 2019; Ishibe et al., 2015; King et al., 1994; Ma et al., 2005; Wang et al., 2017). Our study has confirmed that nonnegligible stress triggering effects with absolute values of calculated ΔCFSs are larger than 0.1 bar on the large earthquakes or nearby active faults from preceding earthquake ruptures in central Taiwan. In addition to earthquake interaction effects among earthquakes in central Taiwan, we explored Coulomb stress effect due to earthquakes located outside of our study area (Chung et al., 2008; Hwang & Kanamori, 1989; Wu et al., 2009; Yu & Liu, 1986) but not far from the Central-Taiwan-Mainshock earthquake sequence at hypocenters of mainshocks in the sequence and eight active faults. Detailed explanation has been included in the supporting information (Text section S1). This Coulomb stress analysis model suggests that only magnitude changes in ΔCFS at hypocenters of mainshocks and along active faults after including additional earthquakes outside of our study area that did not change our conclusion whether mainshocks in the sequence were promoted or not (Tables S4 and S5 and Figures S7 and S8).

However, the mechanism of earthquake triggering by large earthquakes is not the only physical source for triggering earthquakes. For example, postseismic afterslip on the decollement of the fold and thrust belt in central Taiwan had been observed and proposed to release a portion of the cumulative strain (Hsu et al., 2007; Tang et al., 2019). We calculated ΔCFS at hypocenters of subsequent mainshocks in the sequence and on eight active faults due to 14 years of cumulative 1999 postseismic afterslip following the 1999 Chi-Chi earthquake. This Coulomb stress analysis reveals that the 1999 postseismic afterslip did impose significant stress changes at hypocenters of the 2009 Nantou and two 2013 Nantou earthquakes and southern part of flat decollement, CSF, and CCF, which are either larger than 0.1 bar or smaller than −0.1 bar. However, those significant stress changes only lead to magnitude change with no sign change in calculated ΔCFSs, which did not change our conclusion about stress states of mainshocks and nearby fault systems (Text section S2, Table S6, and Figure S9 in the supporting information).

Several studies also proposed other types of earthquake triggering mechanisms, such as low atmospheric pressure during an intense typhoon (Visher, 1924), surface erosional unloading (Steer et al., 2014), even tiny pressure variations related to the diffusing rain water within days to months (Hainzl et al., 2006), radiation of seismic waves (Gomberg et al., 2001), and melting glaciers (Sauber & Molnia, 2004). In future work, we will address the possibility of other triggering mechanisms affects earthquake rupture in central Taiwan. Central Taiwan, a seismically active region, is subject to frequent tropical cyclones and widespread landslides as a consequence of its steep topography. High-quality records of such phenomenon can allow us to explore whether the erosion induced by landslide or the huge rainfall can have potential earthquake triggering effects. Combining stress triggering effects from other mechanisms can deepen our understanding about controlling factors that influence the earthquake generation beyond the long-term tectonic loading.

6. Conclusion

In this study, we investigated triggering effects among 14 strong mainshocks that occurred in central Taiwan from 1900 to 2017 and their impact on 8 nearby fault systems. Our results showed that 5 out of 13 mainshocks were promoted, 7 mainshocks were inhibited to failure, and 1 mainshock (2016 Meinong earthquake) was uncertain whether it was promoted or not when considering all preceding earthquakes with $M_L \geq 5.5$ in central Taiwan. Our Coulomb failure analysis suggest that stress transfer along nearby active fault indicates that preceding earthquakes might trigger the propagation of the 1941 Chungpu, 1998 Rueyli, and 1999 Chi-Chi earthquakes. In addition, preceding earthquakes encourage failures on CKF, CSF, CCF, and FDCT. On the contrary, preceding events inhibit failures on CHF, CLPF, STF, and HHF. Thus, earthquake interaction effects play a vital role in the nucleation and rupture propagation of earthquakes and future rupture of nearby fault systems in central Taiwan over 117-years duration of our study. These stress changes will likely also affect the nucleation and rupture of future earthquakes. Our study suggests that location of mainshock epicenter and its focal depth play a predominant effect in Coulomb failure analysis; influences of source slip models and effective friction coefficient cannot be ignored when receiver fault locates near the source fault, whereas for the case that receiver fault locates far away from source fault, effective friction coefficient plays a dominant effect, and other parameters all have negligible effect. Based on simple statistical analysis of our sensitivity analysis, we suggest a 33–38% uncertainty level in Coulomb stress change calculations when investigating earthquake interaction effects in central Taiwan no matter whether receiver fault is in near field or far field. Our findings also indicate the necessity of investigating other types of earthquake triggering mechanisms considering the complex tectonic environment in central Taiwan.

Acknowledgments

We thank the Editor Yehuda Ben-Zion and two anonymous reviewers for their very constructive reviews. We also thank Yih-Min Wu (National Taiwan University) and Zhigang Peng (Georgia Institute of Technology) for providing the focal mechanism catalog for moderate earthquakes (Tables 1 and S1) used in this study in central Taiwan. This study was supported by NASA (Grant 80NSSC17K0098). This is contribution number 975 from the Southeast Environmental Research Center in the Institute of Environment at Florida International University. Data sets about source faults and receiver faults of the Coulomb stress analyses used in this paper have been archived in https://doi.org/10.6084/m9.figshare.12589443.v1 (Li et al., 2020). All the Coulomb failure models in this paper are conducted through Coulomb 3.3 software (Toda et al., 2005).

References

Asayesh, B. M., Hamzeloo, H., & Zafarani, H. (2019). Coulomb stress changes due to main earthquakes in Southeast Iran during 1981 to 2011. *Journal of Seismology*, *23*(1), 135–150. https://doi.org/10.1007/s10950-018-9797-y

Carena, S., Suppe, J., & Kao, H. (2002). Active detachment of Taiwan illuminated by small earthquakes and its control of first-order topography. *Geology*, *30*(10), 935–938. https://doi.org/10.1130/0091-7613(2002)030<0935:ADOTIB>2.0.CO;2

Catalli, F., & Chan, C.-H. (2012). New insights into the application of the Coulomb model in real-time. *Geophysical Journal International*, *188*(2), 583–599. https://doi.org/10.1111/j.1365-246X.2011.05276.x

Chan, C.-H., & Stein, R. S. (2009). Stress evolution following the 1999 Chi-Chi, Taiwan, earthquake: Consequences for afterslip, relaxation, aftershocks and departures from Omori decay. *Geophysical Journal International*, *177*(1), 179–192. https://doi.org/10.1111/j.1365-246X.2008.04069.x

Chan, C.-H., & Wu, Y.-M. (2012). A seismicity burst following the 2010 M 6.4 Jiashian earthquake—Implications for short-term seismic hazards in southern Taiwan. *Journal of Asian Earth Sciences*, *59*, 231–239. https://doi.org/10.1016/j.jseaes.2012.08.011

Chan, C.-H., & Wu, Y.-M. (2014). Seismic behavior in central Taiwan: Response to stress evolution following the 1999 Mw 7.6 Chi-Chi earthquake. *Journal of Asian Earth Sciences*, *90*, 101–106. https://doi.org/10.1016/j.jseaes.2014.04.006

Chi, W.-C., Dreger, D., & Kaverina, A. (2001). Finite-source modeling of the 1999 Taiwan (Chi-Chi) earthquake derived from a dense strong-motion network. *Bulletin of the Seismological Society of America*, *91*(5), 1144–1157.

Chung, L.-H., Chen, Y.-G., Wu, Y.-M., Shyu, J. B. H., Kuo, Y.-T., & Lin, Y.-N. N. (2008). Seismogenic faults along the major suture of the plate boundary deduced by dislocation modeling of coseismic displacements of the 1951 M7. 3 Hualien–Taitung earthquake sequence in eastern Taiwan. *Earth and Planetary Science Letters*, *269*(3–4), 416–426. https://doi.org/10.1016/j.epsl.2008.02.035

Duan, B., & Oglesby, D. D. (2006). Heterogeneous fault stresses from previous earthquakes and the effect on dynamics of parallel strike-slip faults. *Journal of Geophysical Research: Solid Earth*, *111*, n/a. https://doi.org/10.1029/2005JB004138

Freed, A. M. (2005). Earthquake triggering by static, dynamic, and postseismic stress transfer. *Annual Review of Earth and Planetary Sciences*, *33*(1), 335–367. https://doi.org/10.1146/annurev.earth.33.092203.122505

Gardner, J. K., & Knopoff, L. (1974). Is the sequence of earthquakes in Southern California, with aftershocks removed, Poissonian? *Bulletin of the Seismological Society of America*, *64*(5), 1363–1367.

Gomberg, J., Reasenberg, P. A., & Bodin, P. l, & Harris, R. A. (2001). Earthquake triggering by seismic waves following the Landers and Hector Mine earthquakes. *Nature*, *411*(6836), 462–466. https://doi.org/10.1038/35078053

Hainzl, S., Enescu, B., Cocco, M., Woessner, J., Catalli, F., Wang, R., & Roth, F. (2009). Aftershock modeling based on uncertain stress calculations. *Journal of Geophysical Research: Solid Earth*, *114*, B05S07. https://doi.org/10.1029/2008jb006011

Hainzl, S., Kraft, T., Wassermann, J., Igel, H., & Schmedes, E. (2006). Evidence for rainfall-triggered earthquake activity. *Geophysical Research Letters*, *33*, L19303. https://doi.org/10.1029/2006GL027642

Hough, S. E., Gomberg, J., & Hutton, K. (2002). Remotely Triggered Earthquakes in Southern California? AGUFM, 2002, S72F-1361.

Hsu, Y.-J., Avouac, J.-P., Yu, S.-B., Chang, C.-H., Wu, Y.-M., & Woessner, J. (2009). Spatio-temporal slip, and stress level on the faults within the western foothills of Taiwan: Implications for fault frictional properties. *Pure and Applied Geophysics*, *166*(10–11), 1853–1884. https://doi.org/10.1007/s00024-009-0510-5

Hsu, Y.-J., Rivera, L., Wu, Y.-M., Chang, C.-H., & Kanamori, H. (2010). Spatial heterogeneity of tectonic stress and friction in the crust: New evidence from earthquake focal mechanisms in Taiwan. *Geophysical Journal International*, *182*(1), 329–342.

Hsu, Y.-J., Segall, P., Yu, S.-B., Kuo, L.-C., & Williams, C. A. (2007). Temporal and spatial variations of post-seismic deformation following the 1999 Chi-Chi, Taiwan earthquake. *Geophysical Journal International*, *169*(2), 367–379. https://doi.org/10.1111/j.1365-246X.2006.03310.x
Hsu, Y.-J., Yu, S.-B., Kuo, L.-C., Tsai, Y.-C., & Chen, H.-Y. (2011). Coseismic deformation of the 2010 Jiashian, Taiwan earthquake and implications for fault activities in southwestern Taiwan. *Tectonophysics*, *502*(3–4), 328–335. https://doi.org/10.1016/j.tecto.2011.02.005
Hsu, Y.-J., Yu, S.-B., Loveless, J. P., Bacolcol, T., Solidum, R., Luis, A. Jr., et al. (2016). Interseismic deformation and moment deficit along the Manila subduction zone and the Philippine Fault system. *Journal of Geophysical Research: Solid Earth*, *121*(10), 7639–7665. https://doi.org/10.1002/2016JB013082
Hwang, L. J., & Kanamori, H. (1989). Teleseismic and strong-motion source spectra from two earthquakes in eastern Taiwan. *Bulletin of the Seismological Society of America*, *79*(4), 935–944.
Institute of Earth Sciences, Academia Sinica, Taiwan (1996). *Broadband Array in Taiwan for Seismology*. Taiwan: Institute of Earth Sciences, Academia Sinica, Taiwan. Other/Seismic Network. https://doi.org/10.7914/SN/TW
Ishibe, T., Satake, K., Sakai, S., Shimazaki, K., Tsuruoka, H., Yokota, Y., et al. (2015). Correlation between Coulomb stress imparted by the 2011 Tohoku-Oki earthquake and seismicity rate change in Kanto, Japan. *Geophysical Journal International*, *201*(1), 112–134. https://doi.org/10.1093/gji/ggv001
Johnson, K. M., Hsu, Y.-J., Segall, P., & Yu, S.-B. (2001). Fault geometry and slip distribution of the 1999 Chi-Chi, Taiwan earthquake imaged from inversion of GPS data. *Geophysical Research Letters*, *28*(11), 2285–2288. https://doi.org/10.1029/2000GL012761
Kao, H., Huang, G.-C., & Liu, C.-S. (2000). Transition from oblique subduction to collision in the northern Luzon arc-Taiwan region: Constraints from bathymetry and seismic observations. *Journal of Geophysical Research: Solid Earth*, *105*(B2), 3059–3079. https://doi.org/10.1029/1999JB900357
King, G. C., Stein, R. S., & Lin, J. (1994). Static stress changes and the triggering of earthquakes. *Bulletin of the Seismological Society of America*, *84*(3), 935–953.
Lee, S.-J., Yeh, T.-Y., Huang, H.-H., & Lin, C.-H. (2015). Numerical earthquake models of the 2013 Nantou, Taiwan, earthquake series: Characteristics of source rupture processes, strong ground motions and their tectonic implication. *Journal of Asian Earth Sciences*, *111*, 365–372. https://doi.org/10.1016/j.jseaes.2015.06.031
Li, S., Wdowinski, S., Hsu, Y.-J., & Shyu, J. B. (2020). DataSetsFiles_Paper_2019JB019010R_Earthquake_Interaction_CentralTaiwan (JGR: Solid Earth) (version 1).figshare. https://doi.org/10.6084/m9.figshare.12589443.v1
Liao, B.-Y., & Huang, H.-C. (2016). Coulomb stress changes and seismicity in central Taiwan due to the Nantou blind-thrust earthquakes in 2013. *Journal of Asian Earth Sciences*, *124*, 169–180. https://doi.org/10.1016/j.jseaes.2016.05.001
Liao, Y.-W., Ma, K.-F., Hsieh, M.-C., Cheng, S.-N., Kuo-Chen, H., & Chang, C.-P. (2018). Resolving the 1906 Mw 7.1 Meishan, Taiwan, earthquake from historical seismic records. *Seismological Research Letters*, *89*(4), 1385–1396. https://doi.org/10.1785/0220170285
Lin, D.-H., Chen, K. H., Rau, R.-J., & Hu, J.-C. (2013). The role of a hidden fault in stress triggering: Stress interactions within the 1935 Mw 7.1 Hsinchu–Taichung earthquake sequence in central Taiwan. *Tectonophysics*, *601*, 37–52. https://doi.org/10.1016/j.tecto.2013.04.022
Lin, M., & Xiao, Q. (2004). Seismotectonic model of the Tainan basin, southwestern Taiwan. *Acta Seismologica Sinica*, *17*(4), 447–452. https://doi.org/10.1007/s11589-004-0024-2
Ma, K.-F., Chan, C.-H., & Stein, R. S. (2005). Response of seismicity to Coulomb stress triggers and shadows of the 1999 Mw = 7.6 Chi-Chi, Taiwan, earthquake. *Journal of Geophysical Research: Solid Earth*, *110*, B05S19). https://doi.org/10.1029/2004jb003389
Ma, K.-F., Mori, J., Lee, S.-J., & Yu, S. B. (2001). Spatial and temporal distribution of slip for the 1999 Chi-Chi, Taiwan, earthquake. *Bulletin of the Seismological Society of America*, *91*(5), 1069–1087.
Ma, K.-F., Song, T.-R. A., Lee, S.-J., & Wu, H.-I. (2000). Spatial slip distribution of the September 20, 1999, Chi-Chi, Taiwan, earthquake (Mw7. 6)—Inverted from teleseismic data. *Geophysical Research Letters*, *27*(20), 3417–3420. https://doi.org/10.1029/2000GL011393
Ma, K.-F., & Wu, S. I. (2001). Quick slip distribution determination of moderate to large inland earthquakes using near-source strong motion waveforms. *Earthquake Engineering and Engineering Seismology*, *3*, 1–10.
Mai, P. M., & Thingbaijam, K. K. S. (2014). SRCMOD: An online database of finite-fault rupture models. *Seismological Research Letters*, *85*(6), 1348–1357. https://doi.org/10.1785/0220140077
Meier, M.-A., Werner, M. J., Woessner, J., & Wiemer, S. (2014). A search for evidence of secondary static stress triggering during the 1992 Mw7. 3 Landers, California, earthquake sequence. *Journal of Geophysical Research: Solid Earth*, *119*, 3354–3370. https://doi.org/10.1002/2013JB010385
Mildon, Z. K., Toda, S., Faure Walker, J. P., & Roberts, G. P. (2016). Evaluating models of Coulomb stress transfer: Is variable fault geometry important? *Geophysical Research Letters*, *43*, 12–407. https://doi.org/10.1002/2016gl071128
Mouyen, M., Cattin, R., & Masson, F. (2010). Seismic cycle stress change in western Taiwan over the last 270 years. *Geophysical Research Letters*, *37*, n/a. https://doi.org/10.1029/2009GL042292
Okada, Y. (1992). Internal deformation due to shear and tensile faults in a half-space. *Bulletin of the Seismological Society of America*, *82*(2), 1018–1040.
Price, E. J., & Bürgmann, R. (2002). Interactions between the Landers and Hector Mine, California, earthquakes from space geodesy, boundary element modeling, and time-dependent friction. *Bulletin of the Seismological Society of America*, *92*(4), 1450–1469. https://doi.org/10.1785/0120000924
Sauber, J. M., & Molnia, B. F. (2004). Glacier ice mass fluctuations and fault instability in tectonically active Southern Alaska. *Global and Planetary Change*, *42*(1–4), 279–293. https://doi.org/10.1016/j.gloplacha.2003.11.012
Shyu, J. B. H., Chuang, Y.-R., Chen, Y.-L., Lee, Y.-R., & Cheng, C.-T. (2016). A new on-land seismogenic structure source database from the Taiwan Earthquake Model (TEM) project for seismic hazard analysis of Taiwan. *Terrestrial, Atmospheric and Oceanic Sciences*, *27*(3), 311–323. https://doi.org/10.3319/TAO.2015.11.27.02(TEM)
Shyu, J. B. H., Sieh, K., Chen, Y.-G., & Liu, C.-S. (2005). Neotectonic architecture of Taiwan and its implications for future large earthquakes. *Journal of Geophysical Research: Solid Earth*, *110*, B08402. https://doi.org/10.1029/2004JB003251
Steacy, S., Gomberg, J., & Cocco, M. (2005). Introduction to special section: Stress transfer, earthquake triggering, and time-dependent seismic hazard. *Journal of Geophysical Research: Solid Earth*, *110*, B05S01. https://doi.org/10.1029/2005jb003692
Steer, P., Simoes, M., Cattin, R., & Shyu, J. B. H. (2014). Erosion influences the seismicity of active thrust faults. *Nature Communications*, *5*(1), 5564. https://doi.org/10.1038/ncomms6564
Stein, R. S., King, G. C., & Lin, J. (1992). Change in failure stress on the southern San Andreas fault system caused by the 1992 magnitude = 7.4 Landers earthquake. *Science*, *258*(5086), 1328–1332. https://doi.org/10.1126/science.258.5086.1328
Suppe, J. (1976). Decollement folding in southwestern Taiwan. *Petroleum Geology of Taiwan*, *13*, 25–35.
Suppe, J. (1981). Mechanics of mountain building and metamorphism in Taiwan. *Memoir of Geological Society of China*, *4*(6), 67–89.

10.1029/2019JB019010

Suppe, J., Schaer, J. P., & Rodgers, J. (1987). The active Taiwan mountain belt. *The Anatomy of Mountain Ranges*, 277–293. https://doi.org/10.1515/9781400858644.277

Syed Tabrez, A., Freed, A. M., Calais, E., Manaker, D. M., & McCann, W. R. (2008). Coulomb stress evolution in Northeastern Caribbean over the past 250 years due to coseismic, postseismic and interseismic deformation. *Geophysical Journal International*, *174*(3), 904–918.

Tang, C.-H., Hsu, Y.-J., Barbot, S., Moore, J. D., & Chang, W.-L. (2019). Lower-crustal rheology and thermal gradient in the Taiwan orogenic belt illuminated by the 1999 Chi-Chi earthquake. *Science Advances*, *5*(2), eaav3287.

Toda, S., Stein, R. S., Richards-Dinger, K., & Bozkurt, S. B. (2005). Forecasting the evolution of seismicity in southern California: Animations built on earthquake stress transfer. *Journal of Geophysical Research: Solid Earth*, *110*, B05S16. https://doi.org/10.1029/2004JB003415

Visher, S. S. (1924). Tropical cyclones and earthquakes. *Bulletin of the Seismological Society of America*, *14*(3), 181–184.

Wang, C.-Y., Kuo, S.-Y., Shyu, W.-L., & Hsiao, J.-W. (2003). Investigating near-surface structures under the Changhua fault, west-central Taiwan by the reflection seismic method. *Terrestrial, Atmospheric and Oceanic Sciences*, *14*(3), 343–367. https://doi.org/10.3319/TAO.2003.14.3.343(T)

Wang, J., Xu, C., Freymueller, J. T., & Li, Z. (2017). Probing Coulomb stress triggering effects for a Mw> 6.0 earthquake sequence from 1997 to 2014 along the periphery of the Bayan Har block on the Tibetan Plateau. *Tectonophysics*, *694*, 249–267. https://doi.org/10.1016/j.tecto.2016.11.009

Wang, J., Xu, C., Freymueller, J. T., Li, Z., & Shen, W. (2014). Sensitivity of Coulomb stress change to the parameters of the Coulomb failure model: A case study using the 2008 Mw 7.9 Wenchuan earthquake. *Journal of Geophysical Research: Solid Earth*, *119*, 3371–3392. https://doi.org/10.1002/2012JB009860

Wells, D. L., & Coppersmith, K. J. (1994). New empirical relationships among magnitude, rupture length, rupture width, rupture area, and surface displacement. *Bulletin of the Seismological Society of America*, *84*(4), 974–1002.

Wen, S., Yeh, Y.-L., Chang, Y.-Z., & Chen, C.-H. (2017). The seismogenic process of the 2016 Meinong earthquake, southwest Taiwan. *Terrestrial, Atmospheric and Oceanic Sciences*, *28*(5), 651–662.

Wu, F. T. (1978). Recent tectonics of Taiwan. *Journal of Physics of the Earth*, *26*(Supplement), S265–S299.

Wu, Y.-M., Chang, C.-H., Zhao, L., Shyu, J. B. H., Chen, Y.-G., Sieh, K., & Avouac, J.-P. (2007). Seismic tomography of Taiwan: Improved constraints from a dense network of strong motion stations. *Journal of Geophysical Research: Solid Earth*, *112*, B08312. https://doi.org/10.1029/2007JB004983

Wu, Y.-M., Chang, C.-H., Zhao, L., Teng, T.-L., & Nakamura, M. (2008). A comprehensive relocation of earthquakes in Taiwan from 1991 to 2005. *Bulletin of the Seismological Society of America*, *98*(3), 1471–1481. https://doi.org/10.1785/0120070166

Wu, Y.-M., Zhao, L., Chang, C.-H., Hsiao, N.-C., Chen, Y.-G., & Hsu, S.-K. (2009). Relocation of the 2006 Pingtung earthquake sequence and seismotectonics in southern Taiwan. *Tectonophysics*, *479*(1–2), 19–27. https://doi.org/10.1016/j.tecto.2008.12.001

Wu, Y.-M., Zhao, L., Chang, C.-H., & Hsu, Y.-J. (2008). Focal-mechanism determination in Taiwan by genetic algorithm. *Bulletin of the Seismological Society of America*, *98*(2), 651–661. https://doi.org/10.1785/0120070115

Yu, S.-B., & Liu, C.-C. (1986). Coseismic deformation associated with the May 1986 Hualien earthquake. *Bulletin of the Institute of Earth Sciences, Acadamia Sinica*, *6*, 73–84.

Yue, L.-F., Suppe, J., & Hung, J.-H. (2005). Structural geology of a classic thrust belt earthquake: The 1999 Chi-Chi earthquake Taiwan (Mw = 7.6). *Journal of Structural Geology*, *27*(11), 2058–2083. https://doi.org/10.1016/j.jsg.2005.05.020

Zhan, Z., Jin, B., Wei, S., & Graves, R. W. (2011). Coulomb stress change sensitivity due to variability in mainshock source models and receiving fault parameters: A case study of the 2010–201. Christchurch, New Zealand, earthquakes. *Seismological Research Letters*, *82*(6), 800–814. https://doi.org/10.1785/gssrl.82.6.800

Zhang, W., Iwata, T., Irikura, K., Pitarka, A., & Sekiguchi, H. (2004). Dynamic rupture process of the 1999 Chi-Chi, Taiwan, earthquake. *Geophysical Research Letters*, *31*, L10605. https://doi.org/10.1029/2004GL019827